The Final Report for the DOE Project

Principal Investigator: Xin-Zhong Liang, E-Mail: xliang@umd.edu, Earth System Science Interdisciplinary Center, University of Maryland (UMD), MD20740, http://cwrf.umd.edu

Co-Investigators: Feng Zhang and Shenjian Su, ESSIC/UMD

DOE/Office of Science Program Office: Climate and Environmental Sciences Division

DOE/Office of Science Program Office Technical Contact: Dr. Renu Joseph

Proposal Title: Optimizing the Cloud-Aerosol-Radiation Ensemble Modeling System to Improve Future Climate Change Projections at Regional to Local Scales

Project Period: September 1, 2009 – August 31, 2013

Reporting period: September 1, 2009 – August 31, 2013

SUMMARY FOR PROJECT ACHIEVEMENTS

- We have successfully built up, in consistency and completeness, the Cloud-Aerosol-Radiation (CAR) Ensemble Modeling System. Then we have published the CAR general paper to present a general description of the CAR system and illustrate its capabilities for climate modeling applications, especially in the context of estimating climate sensitivity and uncertainty range caused by cloud-aerosol-radiation interactions. For demonstration purpose, the evaluation is based on several CAR standalone experiments driven by CIRC Phase I data or ERA-Interim observational analysis data (ERI) 2004 global data, and coupled climate model experiments by using CWRF, each comparing a limited subset of the full system ensemble with up to 896 members. It is shown that the quantification of radiative forcings and climate impacts strongly depends on the choices of the cloud, aerosol and radiation schemes. The prevailing schemes used in current GCMs are likely insufficient in variety and physically biased in a significant way. There exists large room for improvement by optimally combining radiation transfer with cloud property schemes.
- We have conducted and published a comprehensive evaluation on the overall accuracy and efficiency of the CAR system among a suite of the alternative schemes that are frequently used in GCMs and RCMs. Two different sets of experiments were conducted. One is the CIRC experiments, i.e., the CIRC Phase I cloudy case data (case 6 and case 7) are used to drive the CAR system, and the other is ERI experiments, i.e., the 6-hourly ERA-Interim observational analysis data (ERI) for January and July 2004 is used to drive the CAR system. In ERI experiments, there are 3 subsets for the evaluation of the overall accuracy for the original raditaion transfer codes, for the evaluation of the overall accuracy for the CAR system and for the effects of cloud subgrid structures, respectively.

These evaluations offer a basic assessment of the CAR's modeling accuracies. Given the range of the best available observations, the CAR ensemble means for TOA and SFC radiative fluxes achieve very good and reasonable accuracies, along with the fact that the model spreads in July wholly cover the observational ranges with ensemble means located in the middles, indicating the successful and robust CAR implementation. This establishes the credibility of the CAR's future wide applications to the climate studies. In addition, the quite large uncertainty ranges are found for cloud radiative forcings (CRFs), implying that these model spreads are dominated by treatments for cloud unresolved structures, cover fractions, top-level positions, particle effective size and optical properties. The calculation accuracies of the original radiation transfer codes can be obviously enhanced by using different cloud schemes including those for cloud cover fraction, particle effective size, water path, and optical properties, and by using better treatments, such as MOSAIC or McICA method, for cloud unresolved structures that can explicitly treat the effects of cloud subgrid variability.

- We have incorporated the CAR into the advanced regional climate model CWRF and published the result of the cloud-aerosol-radiation effects on regional climate modeling along with the CWRF general paper. In CWRF, the CAR system replaces the original WRF radiation driver that consists of the CAM and AER packages, along with the now-obsolete MISC scheme, illustrating one major new feature of the CWRF. It is demonstrated that CWRF has greater application capability and overall better performance than the original WRF. The GSFC radiation (*gsfc*), CSSP surface, and ECP cumulus schemes, newly developed in the CWRF, have certain advantages over their counterparts, producing overall smaller climate biases and better temporal correspondences. Their consistent integration is the key reason for the notable improvement in the downscaling skill of the CWRF over the typical WRF physics configuration and also the well-established CMM5. In addition, Regional climate responses differ substantially among the radiation packages. And the peak frequency occurring more around the zero line indicates that the respective model simulation has more grids of smaller differences from observations and hence is more realistic overall.
- We have conducted and published a study on the key factors to model diversities of cloud radiative effects (CREs) among the seven radiation codes commonly used in the major climate prediction centers worldwide for the first time. In this study, seven sets of global experiments driven by the 6-hourly ERA-Interim observational analysis data (ERI) have been conducted for July 2004, referred to as dcop_dovp1, scop_dovp1, dcop_dovp0, dcop_sovp0, scop_sovp0, scop_sovp1, and gas_exp. Each set has 98 global runs, combining 14 cloud cover members and 7 radiative transfer schemes. It has been found that, after removing the most disagreement in cloud fields, model spreads of CREs among the CAR's seven major radiation schemes, as well as those of radiative fluxes,

dramatically diminish. Taking global mean CREs for example, based on the same 3D distributions of cloud condensates and cover fractions, the current model ranges decreased to <4 Wm^{-2} from about $10Wm^{-2}$ for shortwave and 5-$8Wm^{-2}$ for longwave when using the similar cloud fields among different radiation schemes. Dominant roles of subgrid-scale cloud structures (including vertical overlap and horizontal variability) were demonstrated in general, explaining about 40-75% of the total model spreads. We've also found that model spreads of CREs are very sensitive to cloud cover fractions. Such nonlinear sensitivity can be largely reduced after removing the model difference in the treatments of cloud vertical overlap.

- By using the CAR system, we took part in the AEROCOM project: Intercomparison of shortwave radiative transfer schemes in global aerosol modeling.
- Under the support of this DOE project, we have published five (5) papers in top-rank peer-reviewed journals: ACP (2), JGR (1), BAMS (1), and AAS (1).

Table of Content

1. **Objective as Originally Proposed**

We built a Cloud-Aerosol-Radiation (CAR) ensemble modeling system (Fig. 1) and coupled it with the state-of-the-art mesoscale non-hydrostatic Climate-Weather Research and Forecasting model (CWRF). This system incorporates over 10^{18} versions of numerical representation of interactions among cloud, aerosol, and radiation that are currently available in the literature, including those used by the latest GCMs at NCAR, GFDL, NCEP, NASA, ECMWF and CCCMA. It results from free choices of alternative parameterizations for cloud properties (cover, water, radius, optics, geometry), aerosol properties (type, profile, optics), and radiation transfers (solar, infrared).

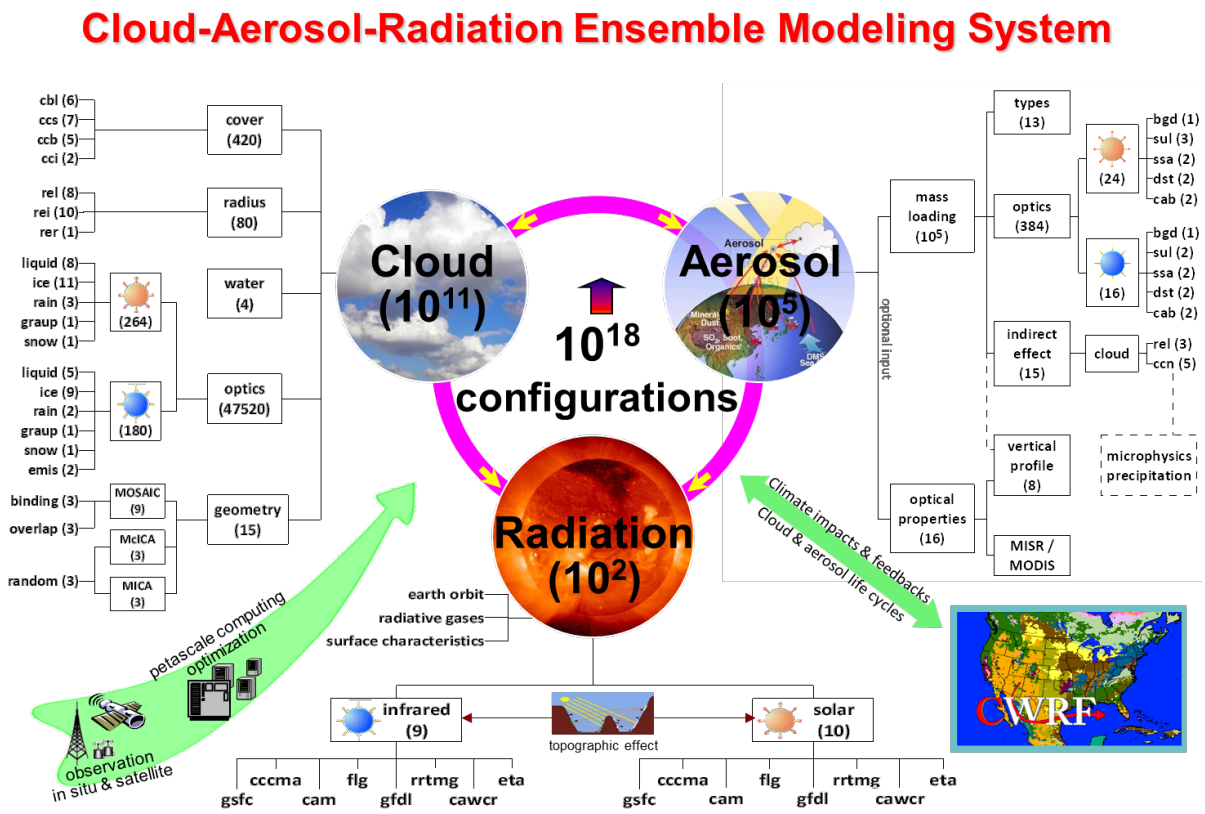

Figure 1 Schematic of the interactive Cloud-Aerosol-Radiation ensemble model (CAR), illustrating all key groups of parameterizations currently available (each with a number of schemes listed in parenthesis) and their links with directional data flow by arrows. Shown also are petascale computing optimization against in situ and satellite observations for ensemble size reduction, as well as the full coupling with CWRF for integration of impacts to and feedbacks from climate variations over the U.S, where the interactive system evaluation is presented in this study.

The full 10^{18} combinations of the CAR system, however, are too massive to be practical, even for the upcoming petascale supercomputing facility. We are utilizing best-available observations (e.g., ARM, ISCCP, SSM/I, MODIS, MISR) to first screen off a significant number of the versions that produce relatively large errors, and then eliminate those that are highly dependent of each other. We anticipate completing this initial phase in another 4 months to reduce the CAR ensemble dimension toward a computationally feasible size. The remaining suite of the versions will form the basis for subsequent ensemble construction and weight optimization, by which CWRF can cost-effectively and most realistically simulate observed cloud-aerosol-radiation interactions and, in general, climate variations and future changes at regional to local scales.

The main objective of this study is to develop a cost-effective CAR ensemble representation to improve climate modeling at regional to local scales. Specifically, we propose to apply CWRF over the U.S. first in a hindcast mode to construct the optimized CAR ensemble that minimizes the model errors in cloud and aerosol properties and radiation fluxes observed during past decades, and then in a predictive mode to project future climate changes in 2050s. The hindcast integrations will be driven by observational reanalyses, while the predictive ones by simulations from NCAR CESM1 at the present and future conditions under IPCC SRES A1Fi (high), A1B (medium) and B1 (low) emissions scenarios. This forcing combination represents the possible range of the uncertainties that result from the likely GCM climate sensitivities under the conceivable emissions scenarios. We will demonstrate that the optimized CWRF-CAR modeling system reduce significantly driving GCMs' present-climate biases and narrows inter-model differences in representing climate sensitivity and hence in simulating the present and future climates at regional to local scales. Given the modular design, the optimized CAR ensemble can be readily transferred to any existing GCMs to improve global climate modeling at ultra-high spatial resolutions. We plan to implement the optimized CAR into the hydrostatic CCSM/CAM3 and demonstrate the skill enhancement at the CWRF resolution (30-km). This CAR should be easily extended to the future non-hydrostatic GCMs.

2. **Abstracts of Publication Acknowledging the Support of the DOE Project**

Under the support of this DOE project, we have published five (5) papers in top-rank peer-reviewed journals. The abstracts for those published papers are presented in this section, while key results will be discussed in the following sections.

a. Liang, X.-Z., and F. Zhang, 2013: The Cloud-Aerosol-Radiation (CAR) ensemble modeling system. *Atmos. Chem. Phys.,* **13**, 8335-8364, doi:10.5194/acp-13-8335-2013.

A Cloud-Aerosol-Radiation (CAR) ensemble modeling system has been developed to incorporate the largest choices of alternate parameterizations for cloud properties (cover, water, radius, optics, geometry), aerosol properties (type, profile, optics), radiation transfers (solar, infrared), and their interactions. These schemes form the most comprehensive collection currently available in the literature, including those used by the world's leading general circulation models (GCMs). The CAR provides a unique framework to determine (via intercomparison across all schemes), reduce (via optimized ensemble simulations), and attribute specific key factors for (via physical process sensitivity analyses) the model discrepancies and uncertainties in representing greenhouse gas, aerosol and cloud radiative forcing effects.

This study presents a general description of the CAR system and illustrates its capabilities for climate modeling applications, especially in the context of estimating climate sensitivity and uncertainty range caused by cloud-aerosol-radiation interactions. For demonstration purposes, the evaluation is based on several CAR standalone and coupled climate model experiments, each comparing a limited subset of the full system ensemble with up to 896 members. It is shown that the quantification of radiative forcings and climate impacts strongly depends on the choices of the cloud, aerosol and radiation schemes. The prevailing schemes used in current GCMs are likely insufficient in variety and physically biased in a significant way. There exists large room for improvement by optimally combining radiation transfer with cloud property schemes.

b. Zhang, F., X.-Z. Liang, Q.-C. Zeng, Y. Gu, and S. Su, 2013: Cloud-Aerosol-Radiation (CAR) ensemble modeling system: Overall accuracy and efficiency. *Adv. Atmos. Sci.*, **30**, 955-973.

The Cloud–Aerosol–Radiation (CAR) ensemble modeling system has recently been built to better understand cloud/aerosol/radiation processes and determine the uncertainties caused by different treatments of cloud/aerosol/radiation in climate models. The CAR system comprises a large scheme collection of cloud, aerosol, and radiation processes available in the literature, including those commonly used by the world's leading GCMs. In this study, detailed analyses of the overall accuracy and efficiency of the CAR system were performed. Despite the different observations used, the overall accuracies of the CAR ensemble means were found to be very good for both shortwave (SW) and longwave (LW) radiation calculations. Taking the percentage errors for July 2004 compared to ISCCP (International Satellite Cloud Climatology Project) data over (60°N, 60°S) as an example, even among the 448 CAR members selected here, those errors of the CAR ensemble means were only about -0.67% (-0.6 W m^{-2}) and -0.82% (-2.0 W m^{-2}) for SW and LW upward fluxes

at the top of atmosphere, and 0.06% (0.1 W m^{-2}) and -2.12% (-7.8 W m^{-2}) for SW and LW downward fluxes at the surface, respectively. Furthermore, model SW frequency distributions in July 2004 covered the observational ranges entirely, with ensemble means located in the middle of the ranges. Moreover, it was found that the accuracy of radiative transfer calculations can be significantly enhanced by using certain combinations of cloud schemes for the cloud cover fraction, particle effective size, water path, and optical properties, along with better explicit treatments for unresolved cloud structures.

c. Zhang, F., X.-Z. Liang, J. Li, and Q.-C. Zeng, 2013: Dominant roles of subgrid-scale cloud structures in model diversity of cloud radiative effects. *J. Geophys. Res.*, **118**, 7733-7749, DOI: 10.1002/jgrd.50604

Today, large model discrepancies exist in estimated cloud radiative effects (CREs) and irradiances across 1-D radiative transfer schemes aimed for climate models. The primary purpose of this study is to understand physical causes of such model discrepancies, especially in CREs under partly cloudy sky. To achieve this goal, the unique Cloud-Aerosol-Radiation (CAR) ensemble modeling system was employed, offline driven by the ERA-Interim global data for July 2004 with no feedback considered. For evaluating each individual contribution from the existing scheme diversity of cloud horizontal inhomogeneity, cloud optical properties, cloud vertical overlap, and gas absorptions, several sets of numerical experiments were conducted. It is the first time to explicitly demonstrate that after removing most of the disagreement in cloud fields, model spreads of CREs among the CAR's seven major radiation schemes, as well as those of radiative fluxes, dramatically diminish. Taking global mean CREs for example, their current model ranges can decrease to < 4 Wm^{-2} from about 10 Wm^{-2} for shortwave and also to < 4 Wm^{-2} from 5–8 Wm^{-2} for longwave. Dominant roles of subgrid-scale cloud structures (including vertical overlap and horizontal variability) were proven in general, explaining about 40–75% of the total model spreads. We have also found that model spreads of CREs are very sensitive to cloud cover fractions. Such nonlinear sensitivity can be largely reduced after removing the model difference in the treatments of cloud vertical overlap.

d. Liang, X.-Z., M. Xu, X. Yuan, T. Ling, H.I. Choi, F. Zhang, L. Chen, S. Liu, S. Su, F. Qiao, J.X.L. Wang, K.E. Kunkel, W. Gao, E. Joseph, V. Morris, T.-W. Yu, J. Dudhia, and J. Michalakes, 2012: Climate-Weather Research and Forecasting Model (CWRF). *Bull. Amer. Meteor. Soc.*, **93**, 1363-1387.

The CWRF has been developed as the Climate extension of the Weather Research and Forecasting model (WRF) by incorporating numerous improvements that are crucial to climate scales, including interactions between land–atmosphere–ocean,

convection–microphysics and cloud–aerosol–radiation, and system consistency throughout all process modules. This extension inherits all WRF functionalities for numerical weather prediction while enhancing the capability for climate modeling. As such, it can be applied for seamless weather forecast and climate prediction. The CWRF has been built with an unprecedentedly comprehensive ensemble of alternative parameterization schemes for each of the key physical processes, including surface (land, ocean), planetary boundary layer, cumulus (deep, shallow), microphysics, cloud, aerosol, and radiation, and their interactions. This facilitates the use of an optimized physics ensemble approach to improve weather or climate prediction along with a reliable uncertainty estimate. The CWRF also emphasizes the societal service capability to provide credible information for climate impacts analyses. For that, it has been coupled with detailed models of terrestrial hydrology, coastal ocean, crop growth, air quality, and recently expanding interactive water quality and ecosystem. Their outputs will form a scientific basis for decision makers to select optimal pathways to achieve economic, societal and environmental goals.

This study provides a general CWRF model description and basic skill evaluation based on a continuous integration for the period 1979-2009 as compared with that of the WRF, using a 30-km grid spacing over a domain including the contiguous U.S. plus southern Canada and northern Mexico. It is demonstrated that the CWRF has greater capability and better performance than the original WRF.

e. Randles C.A., S. Kinne, G. Myhre, M. Schulz, P. Stier, J. Fischer, L. Doppler, E. Highwood, C. Ryder, B. Harris, J. Huttunen, Y. Ma, R. T. Pinker, B. Mayer, D. Neubauer, R. Hitzenberger, L. Oreopoulos, D. Lee, G. Pitari, G. Di Genova, J. Quaas, Fred G. Rose, S. Kato, S. T. Rumbold, I. Vardavas, N. Hatzianastassiou, C. Matsoukas, H. Yu, F. Zhang, H. Zhang, and P. Lu, 2012: Intercomparison of shortwave radiative transfer schemes in global aerosol modeling: Results from the AeroCom radiative transfer experiment. *Atmos. Chem. Phys.*, **13**, 2347-2379, doi: 10.5194/acp-13-2347-2013.

In this study we examine the performance of 31 global model radiative transfer schemes in cloud-free conditions with prescribed gaseous absorbers and no aerosols (Rayleigh atmosphere), with prescribed scattering-only aerosols, and with more absorbing aerosols. Results are compared to benchmark results from high-resolution, multi-angular line-by-line radiation models. For purely scattering aerosols, model bias relative to the line-by-line models in the top-of-the atmosphere aerosol radiative forcing ranges from roughly −10 to 20%, with over- and underestimates of radiative cooling at higher and lower sun elevation, respectively. Inter-model diversity (relative standard deviation) increases from ~10 to 15% as sun elevation increases. Inter-model

diversity in atmospheric and surface forcing decreases with increased aerosol absorption, indicating that the treatment of multiple-scattering is more variable than aerosol absorption in the models considered. Aerosol radiative forcing results from multi-stream models are generally in better agreement with the line-by-line results than the simpler two-stream schemes. Considering radiative fluxes, model performance is generally the same or slightly better than results from previous radiation scheme intercomparisons. However, the inter-model diversity in aerosol radiative forcing remains large, primarily as a result of the treatment of multiple-scattering. Results indicate that global models that estimate aerosol radiative forcing with two-stream radiation schemes may be subject to persistent biases introduced by these schemes, particularly for regional aerosol forcing.

3. The general description of the CAR system, especially for its capabilities in climate modeling applications

Liang, X.-Z., and F. Zhang, 2013: The Cloud-Aerosol-Radiation (CAR) ensemble modeling system. *Atmos. Chem. Phys.,* **13**, 8335-8364, doi:10.5194/acp-13-8335-2013. This was supported by the DOE project and its key results are described below.

In this study, besides the general description of the CAR system, its capabilities in climate modeling applications have been investigated from the following several sides.

(a) Superior of the CAR ensemble system.

By using the input data from the Continual Intercomparison of Radiation Codes (CIRC) (Oreopoulos et al. 2012) overcast cases (i.e., case 6 and case 7), the percentage differences from the LBL reference among various combinations of radiation and cloud SW optical properties schemes (Table 1) have been compared in Table 2.

Table 1 The 7 radiation transfer codes (rad) and 8 SW cloud liquid optical property schemes (swl) in the CAR

rad	7 CAR major radiation transfer schemes: 1 gsfc (Chou and Suarez 1999; Chou et al. 2001) 2 cccma (Li 2002; Li and Barker 2005) 3 cam (Collins et al. 2004) 4 flg (Fu and Liou 1992; Fu et al. 1998; Gu et al. 2011; Liou et al. 2008) 5 gfdl (Schwarzkopf and Ramaswamy 1999; Freidenreich and Ramaswamy 1999) 6 rrtmg (Clough et al. 2005; Iacono et al. 2008; Morcrette et al. 2008) 7 cawcr (Sun and Rikus 1999; Sun 2008)
swl	8 CAR SW cloud liquid optical property schemes: 1 Fu and Liou (1992) 2 Chou and Suarez (1999) 3 Dobbie et al. (1999); Lindner and Li (2000) 4 Hu and Stanmes (1993) look-up tables 5 Kiehl et al. (1996) 6 Chou and Suarez (1999) 7 Slingo (1989) 8 Hu and Stanmes (1993)

Obviously, smallest errors are identified generally not with the default combination of the radiation transfer and cloud optical property schemes in the original packages, except for *gfdl* and *rrtmg* (thick cloud) and *cawcr* (both clouds). For example, in the thick cloud case, scheme 4 (Hu and Stanmes 1993 with look-up tables), 8 (Hu and Stanmes 1993), 4, and 2 (Chou and Suarez 1999) is the best choice respectively for *gsfc*, *cccma*, *cam*, and *flg* radiation transfer, reducing errors of the original cloud scheme by 2-8%. This indicates that the existing radiation packages have large room for improvement by optimal combinations of radiation transfer with cloud property schemes. In addition, no single cloud optical property scheme works best with all radiation transfer schemes and under all cloudy conditions. For example, scheme 5 is the best for *flg*, but not the best for other radiation schemes; scheme 4 combining with *gsfc* is the best for the thick cloud, but the worst for the thin cloud. The performances of cloud optical property schemes assume strong case dependence with some selectiveness to radiation transfer schemes. As a result, to better and fully understand the uncertainties existing in current cloud radiative forcings, some superiors of the ensemble among multiple physical schemes to single one scheme are indicated due to the nonlinear nature of cloud/aerosol/radiation processes.

Table 2 Percentage differences of SWDNS from LBL reference calculations (LBLRTM for LW and CHARTS for SW) among the CAR's major radiation schemes by 8 cloud optical property schemes for CIRC Phase-I case 6 and 7. For each radiation scheme, the smallest error among all cloud schemes is in bold, while the result from the original combination is in parenthesis.

radiation codes	**gsfc**	**cccma**	**cam**	**flg**	**gfdl**	**rrtmg**	**cawcr**
CIRC case 6 (thick cloud, cwp = 263.4 gm^{-2}, LBL = 92.11 Wm^{-2})							
swl1	-11.71	-12.45	-10.53	(-7.50)	-17.68	-8.25	-13.97
swl2	(-1.90)	-2.42	-0.65	-2.88	-8.58	**0.67**	-5.67
swl3	-12.74	(-12.49)	-10.35	-7.13	-18.06	-8.82	-14.99
swl4	**-0.88**	**-2.35**	**-0.56**	2.72	**-7.12**	(2.02)	**(-2.12)**
swl5	-4.54	-4.85	(-2.87)	**0.53**	-10.89	-0.87	-7.61
swl6	(-1.90)	-2.42	-0.65	2.88	-8.58	**0.67**	-5.67
swl7	-6.18	-5.95	-3.86	-3.63	(-10.63)	-3.17	-6.65
swl8	-15.37	-15.44	-13.45	-13.77	-19.61	-14.00	-15.65
CIRC case 7 (thin cloud, cwp = 39.1 gm^{-2}, LBL = 473.69 Wm^{-2})							
swl1	1.01	-3.34	-3.48	(-3.85)	-4.50	-3.27	-5.03
swl2	(5.78)	**1.62**	**1.37**	**0.96**	**0.37**	**1.55**	**-0.61**
swl3	**0.25**	(-4.03)	-4.22	-4.02	-5.13	-3.65	-5.99
swl4	6.55	2.38	2.23	1.20	1.26	(1.90)	(0.73)
swl5	2.28	-1.83	(-2.00)	-2.16	-3.03	-1.56	-3.76
swl6	(5.78)	**1.62**	**1.37**	**0.96**	**0.37**	**1.55**	**-0.61**
swl7	1.55	-2.75	-2.93	-3.43	(-3.72)	-2.86	-3.79
swl8	-0.93	-5.26	-5.44	-5.50	-6.55	-5.66	-6.29

(b) CAR greenhouse gas forcings have been estimated by using the latest IPCC RCPs: future projection of the GHG radiative forcing and hence its climate consequence has a

greater diversity for a higher emission scenario, and meanwhile clouds have large effects on GHG radiative forcing.

This experiment includes simulations of the seven major SW and LW radiation schemes using their original cloud parameterizations (Table 1) for five idealized conditions. All assume the standard midlatitude summer atmospheric profile with no aerosol, surface skin temperature of 294K, solar constant of 1367 Wm^{-2}, solar zenith angle of 53º, and surface albedo of 0.1 and emissivity of 1.0. In addition to a clear sky condition, four overcast cases are considered following *Fu et al.* (1997): high cloud (10-12km) with ice water content (IWC) of 0.0048 gm^{-3} and effective particle size (dei) of 41.5 μm; middle cloud (4-5km) with liquid water content (LWC) of 0.28 gm^{-3} and effective particle radius (rel) of 6.2 μm; low cloud (1-2km) with LWC of 0.22 gm^{-3} and rel of 5.89 μm; all clouds of the above. The only freedom is GHG concentrations, which are specified by the latest IPCC RCPs. They include RCP2.6 (low), RCP4.5 (medium-low), RCP6.0 (medium-high), and RCP8.5 (high) emission scenarios (*Meinshausen et al.* 2011).

Figure 2 compares the CAR outcomes among the seven major radiation schemes for the GHG radiative forcing under each of the four IPCC RCP scenarios, including their mean and min-max range of TOA net SW, LW and total flux change from the pre-industry condition. As the GHG concentration increases from the present to future and from low to high emission scenarios, the mean radiative forcing increases.

On the other hand, the min-max range, or uncertainty due mainly to the treatment of gas absorption differing among the radiation transfer schemes, becomes larger as the GHG concentration increases. The normalized uncertainty of total radiative flux changes is systematically larger under RCP8.5 than RCP4.5, by a factor of 1.04 to 1.11 depending on clear and cloudy conditions in year 2100. This indicates that future projection of the GHG radiative forcing and hence its climate consequence has a greater diversity for a higher emission scenario. Note that *gsfc* and *cam* schemes neglect particular absorbers in the near-infrared spectra, giving zero SW forcing. Thus the results from these two schemes are excluded in the analysis below on the average and spread of SW and total GHG radiative forcing.

Clouds have large effects on GHG radiative forcing. For RCP8.5 in year 2100, the total forcing averaged over all five radiation transfer schemes is 8.11, 9.57, 6.60, 4.82, and 4.19 Wm^{-2} respectively for clear sky and overcast conditions of low-, middle-, high- and all-clouds. The differences result from contrasts in cloud altitude, thickness, and composition. Clouds, most effectively those at high altitudes where temperatures are much colder than at the surface, reduce outgoing LW emission and hence total GHG radiative forcing. An exception is for optically thick low clouds, which produce larger GHG forcing than clear sky as they reflect more SW (for more gaseous absorption in the air above) but emit same LW relative to the surface. The result of all-clouds is close to that of high-clouds because of the dominance

by the LW forcing.

Clouds also alter the spread in GHG radiative forcing calculation. For RCP8.5 in year 2100, the min-max range of the SW forcing across the five radiation transfer schemes is small (0.5 Wm^{-2}) for both clear sky and high cloud (optically thin), while increased to 1.23, 2.26, and 1.08 Wm^{-2} respectively for middle-, low- and all-clouds. Low clouds produce the largest SW forcing inter-model discrepancies, as they are optically thick. In contrast, the LW forcing is determined by vertical differentiation in emitter temperature and absorber optical property. As such, the LW spread is largest (4.27 Wm^{-2}) for clear sky, while reduced to 2.03, 1.51, 2.88 and 0.61 Wm^{-2} respectively for high-, middle-, low- and all-clouds. [The corresponding

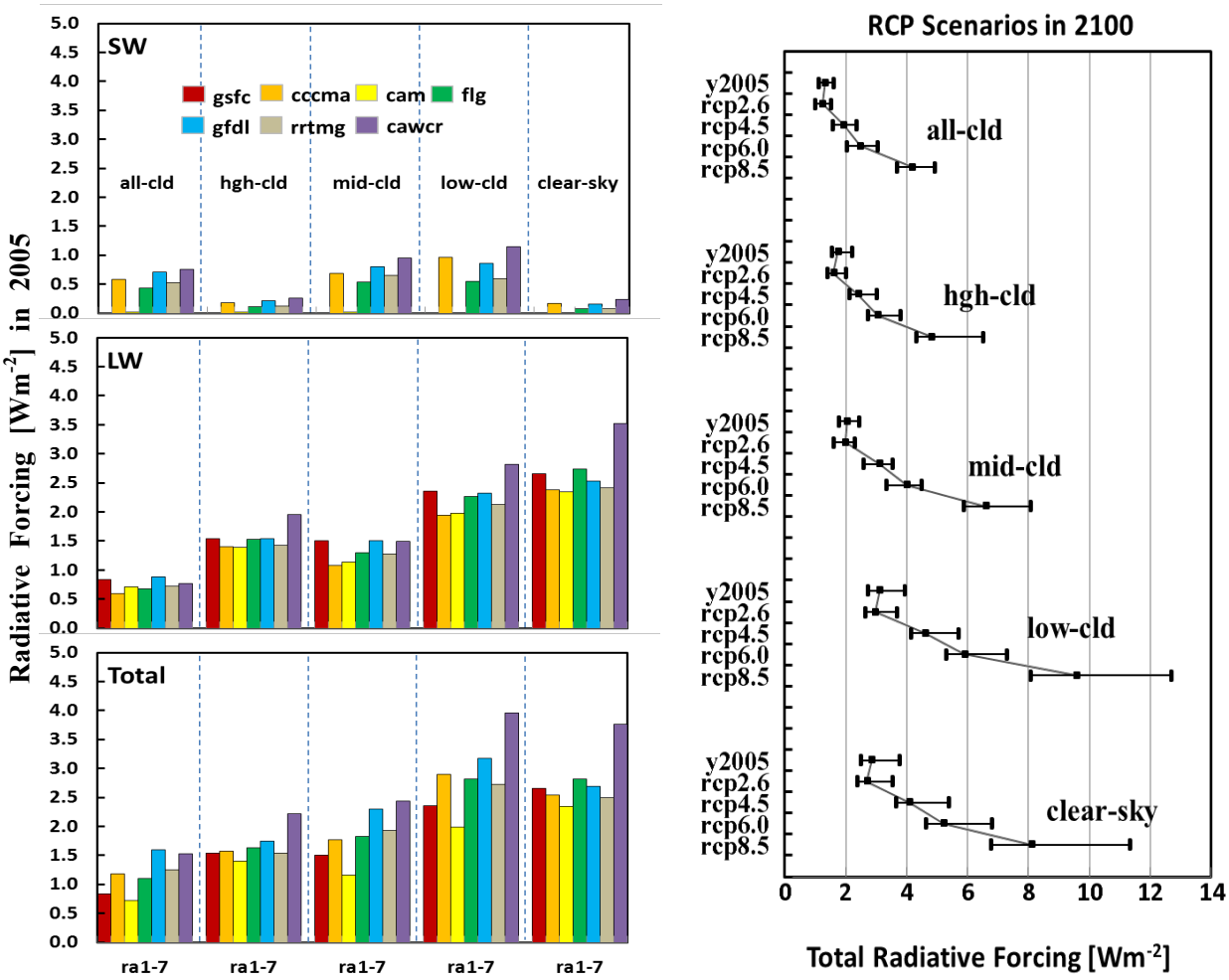

Figure 2 The SW, LW and total radiative forcings (Wm^{-2}) for the present condition in year 2005 among the 7 major radiation transfer schemes (left), and the total radiative forcings (Wm^{-2}) under the clear-sky and prescribed low, middle, high and all cloud conditions for the 4 IPCC RCP scenarios in year 2100 and present conditions (right). Error bars depict the min-max ranges among the radiation transfer schemes excluding gsfc and cam. These forcings are the instantaneous changes in TOA radiative fluxes relative to the aerosol-free condition in year 1765AD without stratospheric adjustment.

values when including *gsfc* and *cam* are respectively 4.37, 2.07, 1.68, 3.22 and 0.61 Wm^{-2}.] Given the dominance of LW effects, clouds tend to decrease the total GHG radiative forcing diversity. One exception, as discussed above, is for low-clouds, which produce a slightly larger total forcing spread than clear sky (4.62 versus 4.55 Wm^{-2}).

(c) CAR aerosol direct radiative effect range is inspected by using the MISR aerosol loading. Clouds reduce aerosol direct effects on TOA and surface radiative fluxes, and the discrepancies of aerosol direct effect that result from radiation and cloud schemes are comparable, and relative to the mean aerosol forcing itself, they are quite large, accounting for 20-30%.

This experiment includes global simulations of the seven major SW radiation schemes along with 64 cloud schemes (four parameterizations each for cover fraction, droplet size, and optical property listed in Table 3) as driven by 6-hourly meteorological conditions during January and July 2004 from the ERA-Interim observational analysis data (ERI) (*Uppala et al.* 2008). The geographic distributions of aerosols were derived from the MISR climatological average over the period 2000-2008 (*Kahn et al.* 2005, 2007).

Table 3 The experiment design for CAR cloud radiative forcing distributions

cloud/radiation components			**schemes selected**
cloud cover fraction		**stratiform (ccs)**	1 Xu and Randall (1996) 2 Slingo (1987)
		cirrus (cci)	2 Slingo (1987)
		boundary (cbl)	1 Slingo (1987)
		deep cumulus (ccb)	3 Slingo (1987) 5 Ferrier et al. (2002)
		total: ctot	1 based on ccs,cci,cbl,ccb
cloud water path (cwp)			2 based on inputted cloud water mass mixing ratio
cloud droplet size		**liquid (rel)**	1 Savijärvi et al. (1997) 3 Min and Harrison (1996)
		ice (dei)	2 Sun and Rikus (1999) 7 Based on air temperature from GFDL
cloud optical property	**LW**	**liquid (lwl)**	2 Chou et al. (2001) 3 Dobbie et al. (1999); Lindner and Li (2000)
		ice (lwi)	106 Fu et al. (1998) 5 Edwards et al. (2007)
	SW	**liquid (swl)**	3 Dobbie et al. (1999); Lindner and Li (2000) 6 Chou and Suarez (1999)
		ice (swi)	106 Fu et al. (1998) 401 Ebert and Curry (1992)
radiation transfer		**LW & SW (rad)**	7 CAR major radiation transfer schemes (Table 1)
total number of experiments			448 each for LW and SW

Figure 3 compares the CAR outcomes among the seven major radiation schemes for the globally averaged total (natural and anthropogenic) aerosol direct effects on SW net radiative fluxes and CRFs at TOA and surface under clear-sky and all-sky conditions among the 64

cloud schemes listed in Table 3, each including its mean and min-max range across the seven major radiation transfer schemes. Shown are the results in July 2004 using the MISR climatological monthly mean aerosol distributions. Clouds reduce aerosol direct effects on TOA and surface radiative fluxes, with their respective full-ensemble mean magnitudes decreased from 4.64 and 6.06 Wm^{-2} in clear-sky to 2.84 and 4.21 Wm^{-2} in all-sky. Such differences of 1.58 and 1.55 Wm^{-2} between clear and all skies represent the SW CRF changes (weakening in both TOA and surface) due to aerosol direct effects. The presence of aerosols, through changes in total optical properties, causes larger reflection in clear-sky and more absorption in clouds, and thus results in a weaker CRF at both TOA and surface.

The above result is in general agreement with the existing estimates. The global ocean

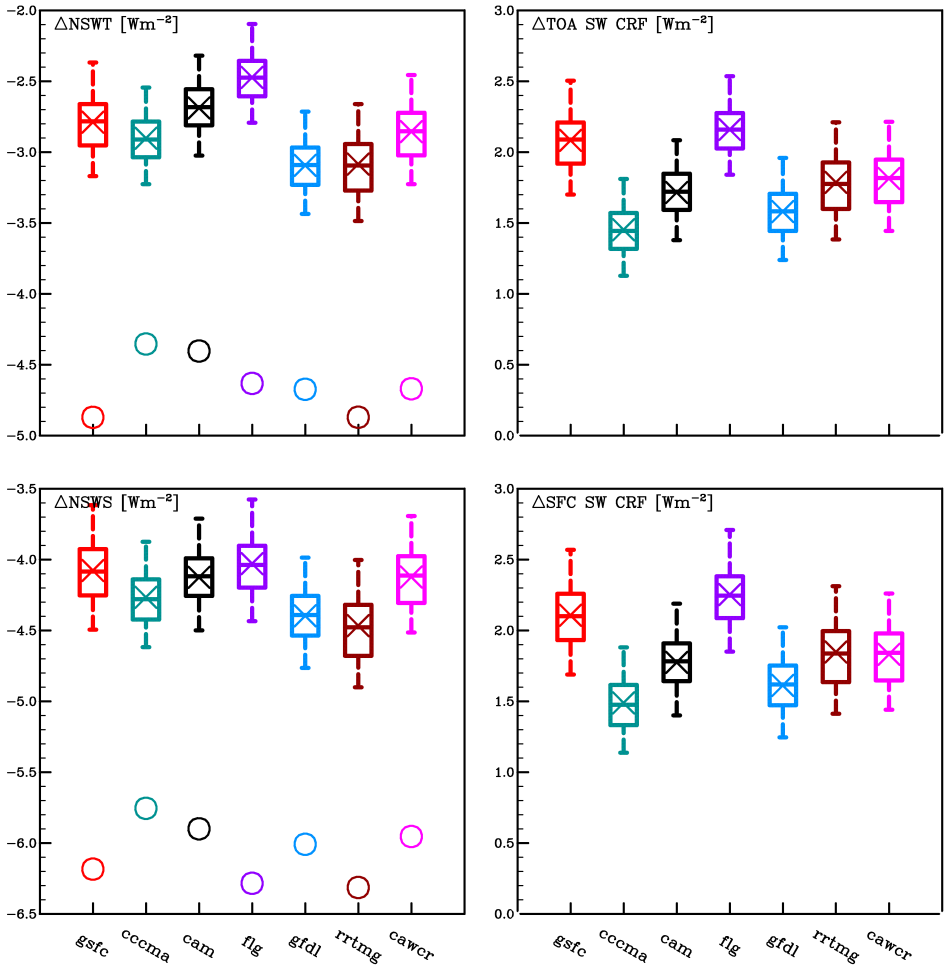

Figure 3 Global mean aerosol direct effects on TOA (*top*) and surface (*bot*) SW all-sky net radiative fluxes (*left*) with clear-sky values (*circle*) and CRFs (*right*) for July 2004 using the MISR climatological aerosol distribution. The box-plot shows the minimum, lower 25% quartile, median, upper 75% quartile, and maximum values among the 64 cloud members for each radiation transfer scheme, while the mark X depicts the ensemble mean.

annual mean clear-sky aerosol direct radiative effect ranges from -6.8 to -3.8 Wm^{-2} based on satellite estimates and from -4.1 to -1.6 Wm^{-2} based on model simulations (Yu et al. 2006; IPCC 2007). The corresponding values averaged in January and July of 2004 from our CAR ensemble, varying from -4.9 to -4.4 Wm^{-2}, fall into the range of the satellite estimates but are more negative than the model simulations. Yu et al. (2006) also used MISR (early version) AOD in combination with GOCART aerosol optical properties to give a global mean estimate of -6.5 Wm^{-2} over ocean and -4.9 Wm^{-2} over land. Our CAR ensemble mean estimate of -4.7 Wm^{-2} over ocean is less negative by ~30%, while that of -4.5 Wm^{-2} over land is very close.

The large difference over ocean could be partly explained by an overall overestimate of 20% (Kahn et al. 2005) in early post-launch MISR AOD retrievals over ocean as used in Yu et al. (2006). Differences in aerosol optical properties and surface albedo between the two studies are among the other contributing factors.

The model outputs for global all-sky aerosol direct effects depend on radiation, cloud, and aerosol schemes. Different radiation schemes simulate aerosol effects, when averaged over the 64 cloud schemes, between negative 2.63-3.21 (4.05-4.44) Wm^{-2} for net SW fluxes and positive 1.23-1.84 (1.27-1.92) Wm^{-2} for CRF at TOA (surface). Thus the discrepancies for these variables due to the choice of radiation scheme are about 0.58 (0.39) and 0.61 (0.65) Wm^{-2}, respectively. The corresponding discrepancies due to the choice of cloud schemes, as depicted by the min-max ranges of individual radiation schemes, are 0.61-0.72 (0.66-0.78) and 0.60-0.72 (0.66-0.78) Wm^{-2}, respectively. Therefore, the discrepancies that result from radiation and cloud schemes are comparable, and relative to the mean aerosol forcing itself, they are quite large, accounting for 20-30%.

4. The overall accuracy and efficiency of the CAR system

Zhang, F., X.-Z. Liang, Q.-C. Zeng, Y. Gu, and S. Su, 2013: Cloud-Aerosol-Radiation (CAR) ensemble modeling system: Overall accuracy and efficiency. *Adv. Atmos. Sci.*, **30**, 955-973. This was supported by the DOE project and its key results are described below.

This study is focused on the evaluation of the CAR, a new platform for climate studies related to cloud/aerosol/radiation processes. The overall accuracy and efficiency analyses and some discussions on how to further improve the accuracy of radiation transfer calculations, especially under cloudy sky, are presented. The cloud schemes used by the CAR original radiation transfer codes are shown in Table 4.

In this study, two different sets of experiments were conducted using a suite of the alternative schemes that are frequently used in modern GCMs (General Circulation Models) and RCMs (Regional Climate Models). Details are as follows:

(a) CIRC experiments. The result indicates that the existing radiation packages have large room for improvement by optimal combinations of radiation transfer with cloud property schemes.

The CIRC Phase I cloudy case data (Oreopoulos and Mlawer 2010; Oreopoulos et al. 2012), i.e., case 6 and case 7, are used to drive the CAR system. Note that gas concentrations, aerosol single scattering properties, cloud water path and effective particle size, surface albedo (unweighted spectral) and emissivity are specified by the CIRC standard. The only freedom is the choice for cloud liquid optical property schemes (Table 1). The outcomes are compared with the line-by-line (LBL) reference results available by CIRC to evaluate the accuracy of various radiation transfer schemes with different cloud liquid optical property parameterization used.

Similar to equation (4) in Oreopoulos et al. (2012), we define the total percentage difference $e_{tot}(\%)$ from the LBL references (SW: LBLRTM-CHARTS) that accounts for different flux types as follows: $e_{tot}(\%) = 0.5\times(|e_{SWDNS,\%}| + |e_{SWUPT,\%}|)$, where $e_{SWDNS,\%}$, and $e_{SWUPT,\%}$ are the % difference of SWDNS (SW downward radiative fluxes at SFC) and SWUPT (SW upward radiative fluxes at TOA) from the LBL references provided

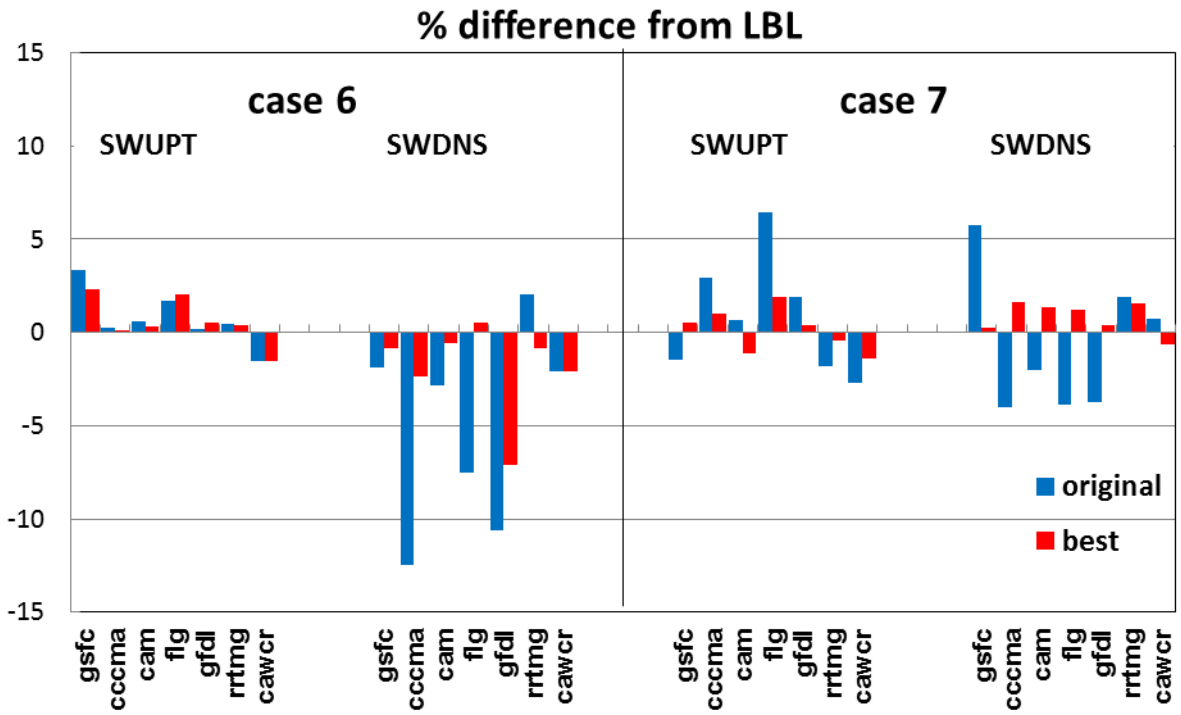

Figure 4. The percentage difference (%) of SWUPT and SWDNS from the LBL reference (LBLRTM-CHARTS) for CIRC phase-I case 6~7. Here, two results from 7 CAR major radiation codes are shown: one, results for those with original cloud optical property scheme used (*blue bars*); the other, the best results assuming the smallest $e_{tot}(\%)$ among the 8 swls (*red bars*).

Table 4. The cloud schemes[1] used by the CAR original radiation transfer codes

rad	treatment for unresolved cloud structure	rel[2]	dei[3]	lwl	lwi	swl	swi
gsfc	max/random overlap of homogeneous clouds	Szczodrak et al. 2001	McFarquhar 2000	Chou et al. 2001	Chou et al. 2001	Chou and Suarez 1999	Chou and Suarez 1999
cccma	McICA method of inhomogeneous clouds	Szczodrak et al. 2001	McFarquhar 2000	Dobbie et al. 1999; Lindner and Li 2000	Fu et al. 1998	Dobbie et al. 1999; Lindner and Li 2000	Fu et al. 1998
cam	max/random overlap of homogeneous clouds	Kiehl et al. 1996	Kristjässon et al. 1999	a constant extinction coefficient used	Ebert and curry 1992	Kiehl et al. 1996	Kiehl et al. 1996
flg[4]	max/random overlap of homogeneous clouds	Szczodrak et al. 2001	Gu and Liou 2006; Liou et al. 2008	Fu and Liou 1993	Fu et al. 1998	Fu and Liou 1993	Fu et al. 1998
gfdl	McICA method of inhomogeneous clouds	Szczodrak et al. 2001	Based on air temperature	Fu and Liou 1993	Fu and Liou 1993	Slingo 1989	Fu 1996
rrtmg	McICA method of homogeneous clouds	Szczodrak et al. 2001	McFarquhar 2000	Hu and Stanmes 1993 look-up tables	Key 2001	Hu and Stanmes 1993 look-up tables	Key 2001
cawcr	max/random overlap of homogeneous clouds	Szczodrak et al. 2001	McFarquhar 2000	Hu and Stanmes 1993 look-up tables	Edwards et al. 2007	Hu and Stanmes 1993	Edwards et al. 2007

here,

rad: radiation transfer scheme; rel: scheme for cloud liquid droplet effective radius; dei: scheme for cloud ice particle effective size
lwl: scheme for cloud liquid water LW optical properties; lwi: scheme for cloud ice water LW optical properties;
swl: scheme for cloud liquid water SW optical properties; swi: scheme for cloud ice water SW optical properties

Note:

by CIRC. Figure 4 compares the $e_{SWDNS,\%}$ and $e_{SWUPT,\%}$ between the results of the original radiation codes (called original here, *blue bars*. Please refer to Table 4 for the original swl) and the best results assuming the smallest $e_{tot}(\%)$ among the 8 swl schemes (Table 1) (called best, *red bars*) for CIRC case 6 and 7.

The $e_{SWDNS,\%}$ and $e_{SWUPT,\%}$ of the original radiation codes are among -12.5~6.5%, which lie in the ranges disclosed by Oreopoulos et al. (2012). However, the obvious differences between the blue and red bars indicate that the original radiation codes don't always generate the best results. By using different cloud liquid optical property schemes, most % differences of SWUPT and SWDNS from LBL can be decreased by a factor of 1.22 ~ 23.41, depending on cases and radiation codes. The smallest % differences for these two CIRC cloudy cases are generally within ±2.5%, showing very good accuracies. Therefore, even when the same cloud droplet sizes and the same cloud water path are used, the complexity of cloud optical property treatments is one uncertain factor for the solar radiation transfer calculations.

(b) ERI experiments

The 6-hourly ERA-Interim observational analysis data (ERI, Uppala et al. 2008) for January and July 2004 is used to drive the CAR system. The cloud water path is directly calculated from the inputted cloud water mass mixing ratio. MISR climatological mean aerosol optical properties over the period 2000-2008 (Kahn et al. 2005, 2007) are used to account for the aerosol direct effects. Although only two months are evaluated here, the statistics over [60ºS, 60ºN] have included about 10^5 cloudy columns over the globe, which assumes sufficient clouds in variety for this study.

Overall accuracy for the CAR system. Despite the different observations used, the overall accuracies of the CAR ensemble means are very good for both shortwave (SW) and longwave (LW) radiation calculations. And the existing radiation packages have large room for improvement by optimal combinations of radiation transfer with cloud schemes.

To evaluate the CAR system's overall accuracy, the global simulations using the CAR 7 major radiation schemes, each combining with the 64 cloud members listed in Table 3, are designed. In total, 448 runs were made for both LW and SW.

Figure 5 illustrates the boxplot of *%bias* of 448 CAR members from different observations for July (2004) mean all-sky SWUPT, SWDNS, LWUPT, LWDNS. The calculation is based on all 1.5° grids over [60°S, 60°N]. Despite the large spread among these 448 CAR members, the ensemble means of *%bias* compared to each of these observations chosen here are within -0.67 ~ 8.59% (-0.6 ~ 8.2 Wm^{-2}) for SWUPT, -5.34 ~ 0.06% (-10.4 ~ 0.1 Wm^{-2}) for SWDNS, -2.40 ~ -0.82% (-5.7 ~ -2.0 Wm^{-2}) for LWUPT, and -2.12 ~ -1.55%

(-7.8 ~ -5.7 Wm^{-2}) for LWDNS. The CAR ensemble means get very good overall accuracies for both SW and LW radiation calculations, establishing the credibility of the CAR's future climate applications in climate models. Similar results are gotten for January 2004 (not shown). In addition, using ISCCP as the reference usually generates the smallest *%bias*, while the largest *%bias* is from the CERES, especially for SW. The ensemble means of %*bias* from ISCCP are only about -0.67% (-0.6 Wm^{-2}), 0.06% (0.1 Wm^{-2}), -0.82% (-2.0 Wm^{-2}) and -2.12% (-7.8Wm^{-2}) for SWUPT, SWDNS, LWUPT, and LWDNS, respectively. This strange phenomenon maybe indicates that the schemes chosen in this study are not enough in variety, or the schemes chosen here are improperly tuned toward ISCCP, or the cloud water fields are closest to those from ISCCP.

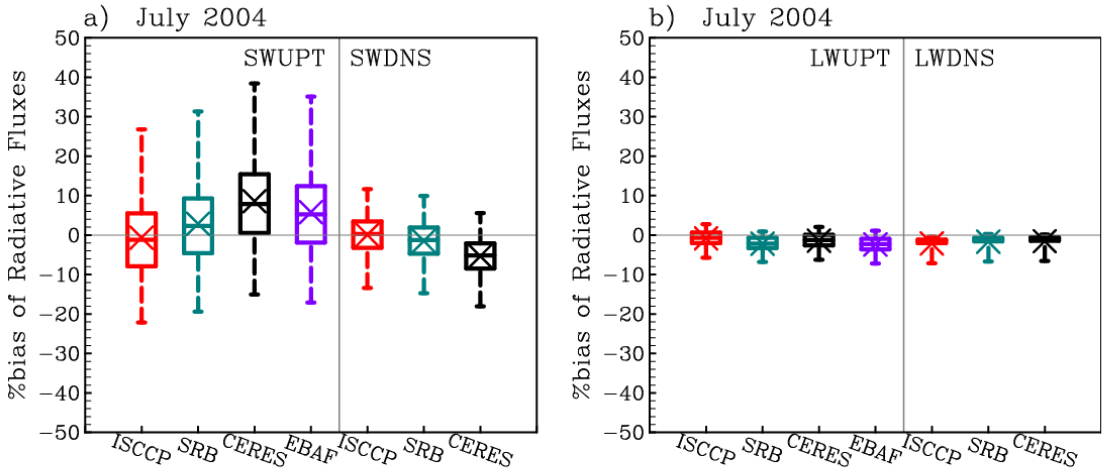

Figure 5. The boxplot of *%bias* from different observations for July (2004) mean all-sky SWUPT, SWDNS, LWUPT, LWDNS for 448 CAR members. EBAF is CERES_EBAF. For each observation, the min, 25% quartile, median, 75% quartile, and max values among 448 CAR members are shown. The averaged among these 448 CAR members are also shown by mark X.

To better show the CAR's great potential to improve the radiation transfer calculation accuracies, the total $\overline{\%rmse}$ from ISCCP with those for the original radiation transfer codes (Table 4, depicted by the mark X) are shown in Figure 6. Here $Total\ \%rmse = 0.5 * (\%rmse_{UPT} + \%rmse_{DNS})$. Similar *rmse* results are shown for different observations, so only those from ISCCP are taken as an example here. For all radiation transfer schemes except *flg* and *cccma*, generally >25% (> 16) of CAR cloud members have smaller SW $\overline{\%rmse}$ than those for the original radiation codes, implying that although original radiation transfer codes have quite good accuracies, there still exists some room to improve them by applying better cloud scheme combinations. For example, for July (2004) means, among the 64 CAR cloud members selected here, the smallest total %*rmses* of SWDNS for *gsfc*, *cam*, *gfdl*, *rrtmg*, and *cawcr* are 20.79%, 21.07%, 21.16%, 20.78%, and 21.13%, while the

corresponding total *%rmses* for the original radiation transfer codes are 23.86%, 21.96%, 22.64%, 22.24%, and 23.76%, respectively. About 1% ~ 3% decreases in *%rmses* are found for these radiation transfer schemes by using different cloud scheme combinations. And if we remove those worse than the originals, the ensemble means are, for sure, better than the originals. All of these emphasize the large SW errors emerging from the treatments of cloud cover fractions, particle effective sizes, and optical properties. Meanwhile the better accuracies of the original *flg* and *cccma* SW calculations and almost all better original LW calculations than those for the 64 CAR cloud members may indicate the insufficient schemes chosen in this study. Undoubtedly, in near future, we should include and investigate as many CAR cloud members as possible. And to get better ensembles of the CAR, at first, the outliers will be deleted, and then based on what remain, we will try to find

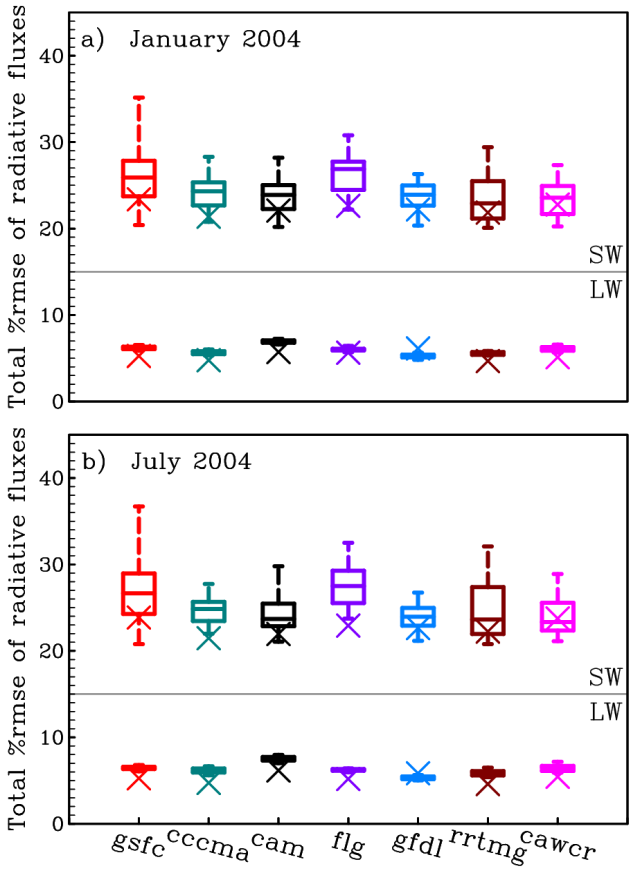

Figure 6. The boxplot of total *%rmse* from ISCCP for January and July 2004 mean all-sky SW and LW radiative fluxes for each radiation schemes with the min, 25% quartile, median, 75% quartile, and max values among 64 CAR cloud members shown. The mark X depicts the results from the original radiation transfer codes. Here $Total\ \%rmse = 0.5 * (\%rmse_{UPT} + \%rmse_{DNS}), \%rmse = rmse/\overline{O}$, $rmse$ is the model spatial root mean square error, $\overline{O}$ the observed domain mean, and the calculation is based on all 1.5° grids over [60°S, 60°N]. *UPT* and *DNS* are upward and downward fluxes at TOA and SFC, respectively.

the normal distributions of the problems of interest. Finally the better performances of the CAR ensembles, e.g., than those of the original ones, are expected.

Effects of cloud subgrid structures. Compared with the conventional treatments (maximum/random cloud overlap), the McICA treatment obviously reduces the *rmse*s of TOA and SFC SW CRFs, especially for *gsfc*.

The effects of the vertical overlap treatments of inhomogeneous clouds on radiative transfer calculations have also been investigated using the CAR. In the original radiation transfer codes, the maximum/random overlap among high/middle/low cloud blocks is adopted by *gsfc* and *flg*, while the maximum/random overlap among adjacent/non-adjacent layers is applied by *cam* and *cawcr*. The other three radiation transfer codes, i.e., *cccma*, *gfdl*, and *rrtmg*, employ McICA treatments with different random cloud generators.

Figure 7 shows the *rmse* of SW SFC and TOA CRFs (*left*) and *%rmse* for all-sky SWUPT and SWDNS (*right*) for July 2004 from ISCCP observations. The same set of schemes for cloud cover fraction, particle effective size, and optical properties is applied for each radiation transfer scheme. Besides the results from the radiation schemes with original overlap treatments (called original here, *blue bars*), the results for those with the same McICA treatment (called McICA, *red bars*) are also shown. The only differences among original and McICA ones are the different treatments for the vertical overlap of inhomogeneous clouds. For *gsfc*, *cam*, *flg*, and *cawcr*, different implementations of the same maximum/random overlap approximation generate quite large discrepancy of CRFs with values about 15Wm^{-2}, comparable with those found in Barker et al. (2003). Compared with the conventional treatments (maximum/random cloud overlap), the McICA treatment obviously reduces the *rmse*s of TOA and SFC SW CRFs, especially for *gsfc*. The *rmse*s for *gsfc* decrease by about 15 Wm^{-2} from about 38Wm^{-2} to 23Wm^{-2}, and accordingly, the corresponding *%rmses* of SWUPT and SWDNS reduce from about 42% to ~28%, and from about 22% to <18%, respectively. While for *cccma*, *gfdl*, and *rrtmg*, the relatively smaller differences between the original and the McICA are mainly due to the different random cloud generator used. In most current GCM radiation schemes, maximum/random overlap of homogeneous clouds with different implementation is assumed (Barker et al. 2003). Hence the vertical overlap treatments of inhomogeneous clouds should be another major uncertain factor influencing the current radiation transfer calculations. When different observation (CERES or SRB) is used, the same conclusions are reached (not shown).

We also note that besides the same cloud optical properties and cloud cover fraction used, when the same McICA treatment is consistently applied to each CAR major radiation transfer code, the *rmse*s of TOA and SFC radiation fluxes are similar with each other. This is mainly due to the smaller differences among different radiation transfer codes when the same cloud structure is used (Liang and Zhang 2013, ACP, soon to be submitted), indicating the

importance of cloud subgrid structures in the simulation of radiation field. Similar results are gotten for other observations, e.g., CERES, SRB (not shown). The remaining errors are from the insufficient treatments of cloud cover fraction, water path, particle effective size, and optical properties, accompanying with those inadequate schemes for aerosol and gas absorptions.

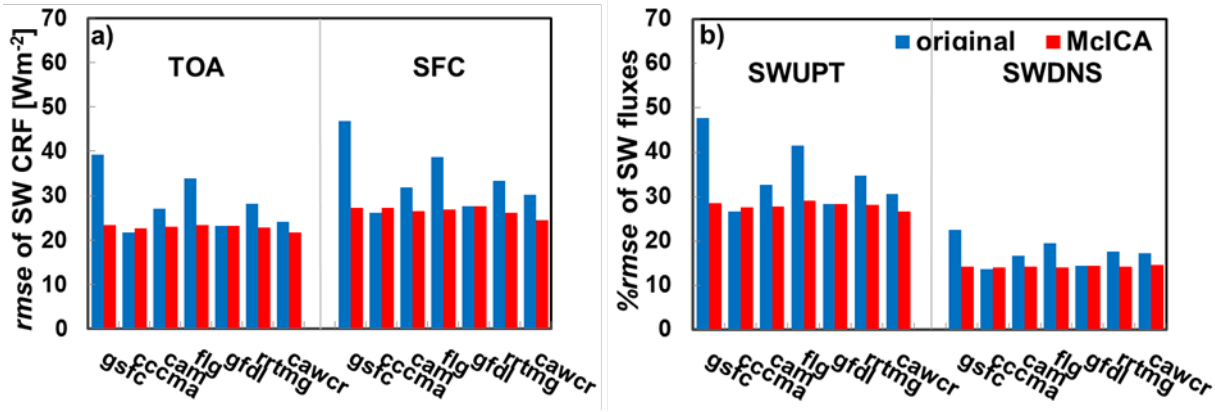

Figure 7. The *rmse* of SW SFC and TOA CRFs (*left*) and *%rmse* for SWUPT and SWDNS under all sky for July 2004 over [60°S, 60°N]. Here $\%rmse = rmse/\overline{O}$, where *rmse* is the model spatial root mean square error, $\overline{O}$ the ISCCP data. Note that only one scheme set for cloud cover fraction, particle effective size and optical properties is used.

Computational Efficiency of the CAR. The CPU efficiencies are quite different among different radiation transfer schemes. The radiation driver takes over 95%, in which about 5% - 20% is used by the two couplers and the rest (70-90%) by the radiative transfer part alone.

In order to fully evaluate the computational efficiency of the major parts of the CAR by including as many as cloud/aerosol schemes, 1-day global runs for total 21 CAR members have been carried out. These 21 CAR members designed here have different cloud-aerosol combinations, which fully cover all alternative cloud/aerosol schemes that can be offline used for ccs (7), ccb (2), cbl (3), cwp (4), rel (6), dei (11), swl (8), swi (18), swr (3, schemes for SW cloud rain), lwl (5), lwi (16), lwr (2, schemes for LW cloud rain) and aerosol (3) schemes. Each of the 7 major radiation transfer schemes is randomly applied three times among these 21 CAR combinations. These experiments are driven by the ERI global data used above at the NERSC's hopper system without parallel calculations. The total time cost by these experiments is about 14637 seconds (> 4 hours), which is enough for us to diagnose the computational efficiency of each part of the CAR.

Figure 8 (a) illustrates the computational efficiency of each radiation transfer package as compared with *cawcr*. Clearly the CPU efficiencies are quite different among different

radiation transfer schemes. The *cawcr* assumes the best CPU efficiency because some of its spectra-dependent coefficients are prepared in advance and read only once by its initial program. The CPU efficiencies of *cccma*, *gfdl* and *rrtmg* are close to *cawcr*. The time consumed by *gsfc* is twice that by *cawcr*. And note that *flg* has the lowest CPU efficiency, about 11 times slower than *cawcr*. This is just due to the delta-four-stream method for SW and the combined delta-four-and-two stream method for LW are used in *flg*, while the other schemes apply the delta-two-stream or Eddington methods.

Figure 8 (b) shows the CPU time partition among the major parts of the CAR system. Clearly the CAR system has a unique advantage in the structured CPU time distribution. The rad_ext, cloud and aerosol drivers consume less than 5%, while the radiation driver takes over 95%, in which about 5% - 20% is used by the two couplers and the rest (70-90%) by the radiative transfer part alone. Due to the small percentage in the total time consumed, the differences in CPU among different cloud or aerosol schemes are negligible. So for the calculations of radiative fluxes and heating rates, the radiative transfer part, producing relatively smaller differences, especially when the same cloud properties including the same cloud subgrid structures are used, is most expensive, however, the cloud and aerosol drivers plus the two couplers, contributing most of the sensitivities, are quite efficient. Hence just

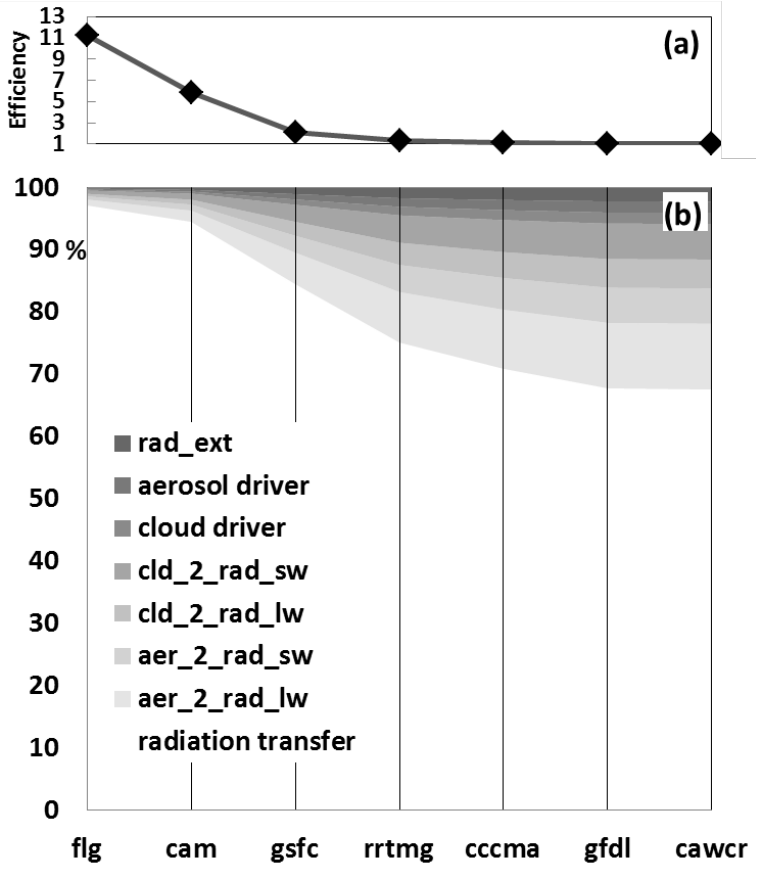

Figure 8. (a) The computational efficiency of each radiation transfer package as compared with cawcr; (b) CPU time partition among the major parts of the CAR system.

based on 1~3 radiation transfer schemes, by comparing the inexpensive yet great variable part (over 10^{16} variations), we can fully evaluate the uncertainty range caused by different treatments for cloud and aerosol physical and optical properties in climate models.

5. The performance of CAR in the CWRF

Liang, X.-Z., M. Xu, X. Yuan, T. Ling, H.I. Choi, F. Zhang, L. Chen, S. Liu, S. Su, F. Qiao, J.X.L. Wang, K.E. Kunkel, W. Gao, E. Joseph, V. Morris, T.-W. Yu, J. Dudhia, and J. Michalakes, 2012: Climate-Weather Research and Forecasting Model (CWRF). *Bull. Amer. Meteor. Soc.*, **93**, 1363-1387. This was partially supported by the DOE project and its key results related to CAR are described below.

(a) The CAR system is one of the major new features of the CWRF (Figure 9).

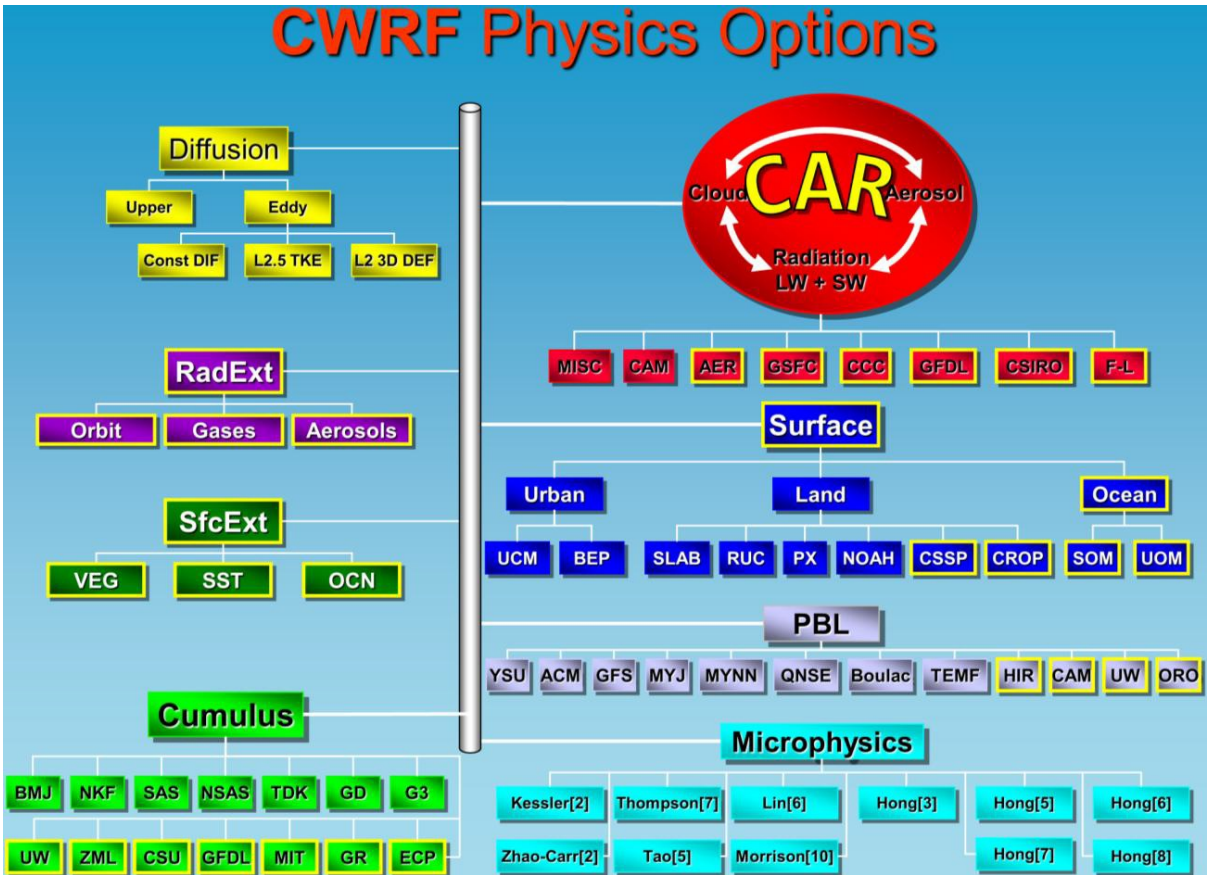

Figure 9. The schematic of the current CWRF physics options and executing sequence from the top down. The CAR ensemble system and all modules or schemes outlined in yellow are additions specifically developed for the CWRF, while others are inherited from the WRF.

(b) The good performance of the CWRF with default physical configures. The GSFC *radiation (gsfc)*, CSSP *surface*, and ECP *cumulus* schemes, newly developed in the

CWRF, have certain advantages over their counterparts, producing overall smaller climate biases and better temporal correspondences.

Figure 10 compare the corresponding biases (simulations minus observations) between the RCMs for downwelling shortwave radiation flux. Shortwave radiation is substantially overestimated over most land by the CMM5, WRFG, and WRF, especially in spring and summer with excess of 30-60 Wm^{-2}. The CWRF, however, produces a much more realistic simulation, mostly within ±20 Wm^{-2}. Nonetheless, the GSFC *radiation (gsfc)*, CSSP *surface*, and ECP *cumulus* schemes, newly developed in the CWRF, have certain advantages over their counterparts, producing overall smaller climate biases and better temporal correspondences. Their consistent integration is the key reason for the notable improvement in the downscaling skill of the CWRF over the typical WRF physics configuration and also the well-established CMM5.

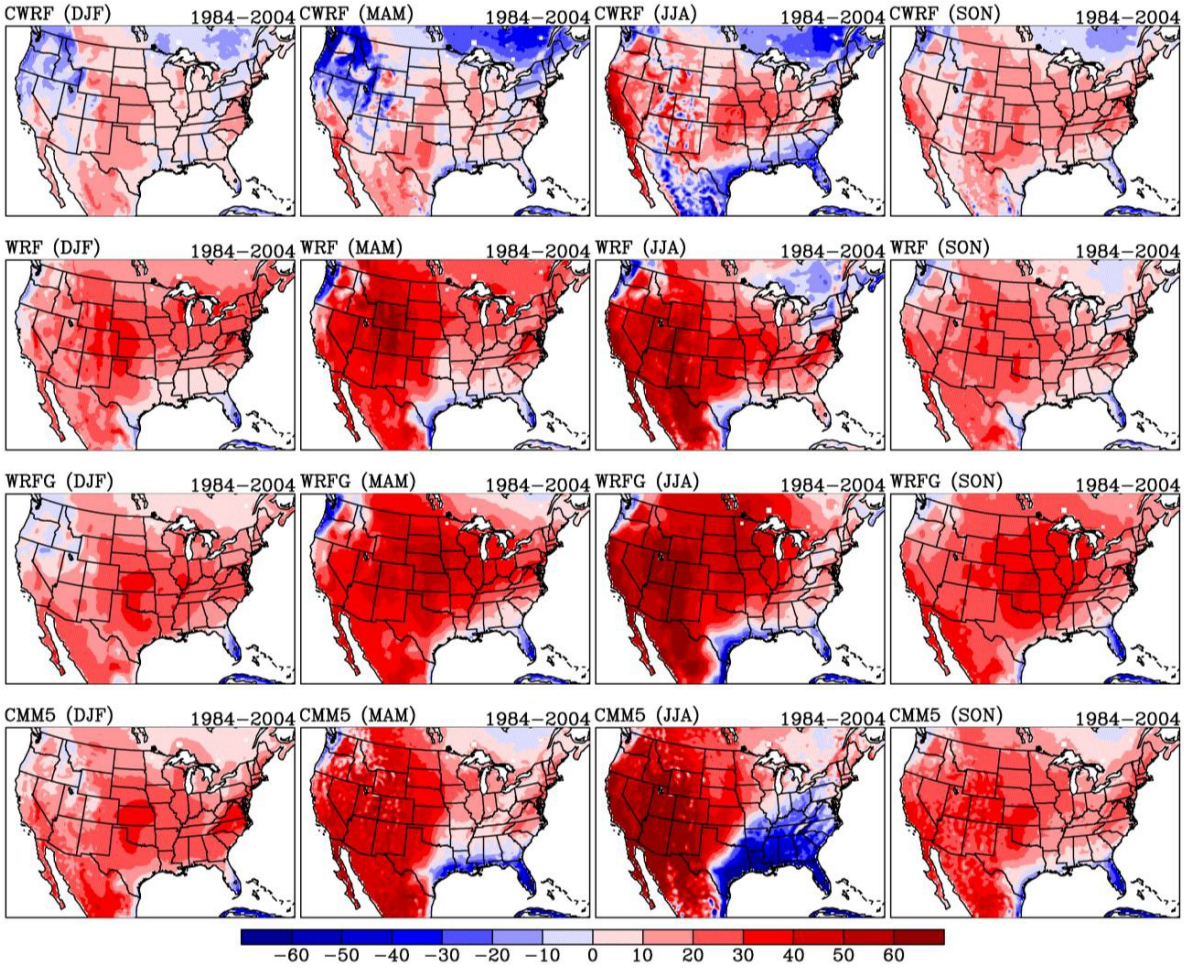

Figure 10. The geographic distributions of seasonal (DJF, MAM, JJA, SON) mean surface downwelling shortwave radiation flux ($W\ m^{-2}$) biases (departures from observations) averaged during 1984-2004 as simulated by the CWRF, WRF, WRFG, and CMM5.

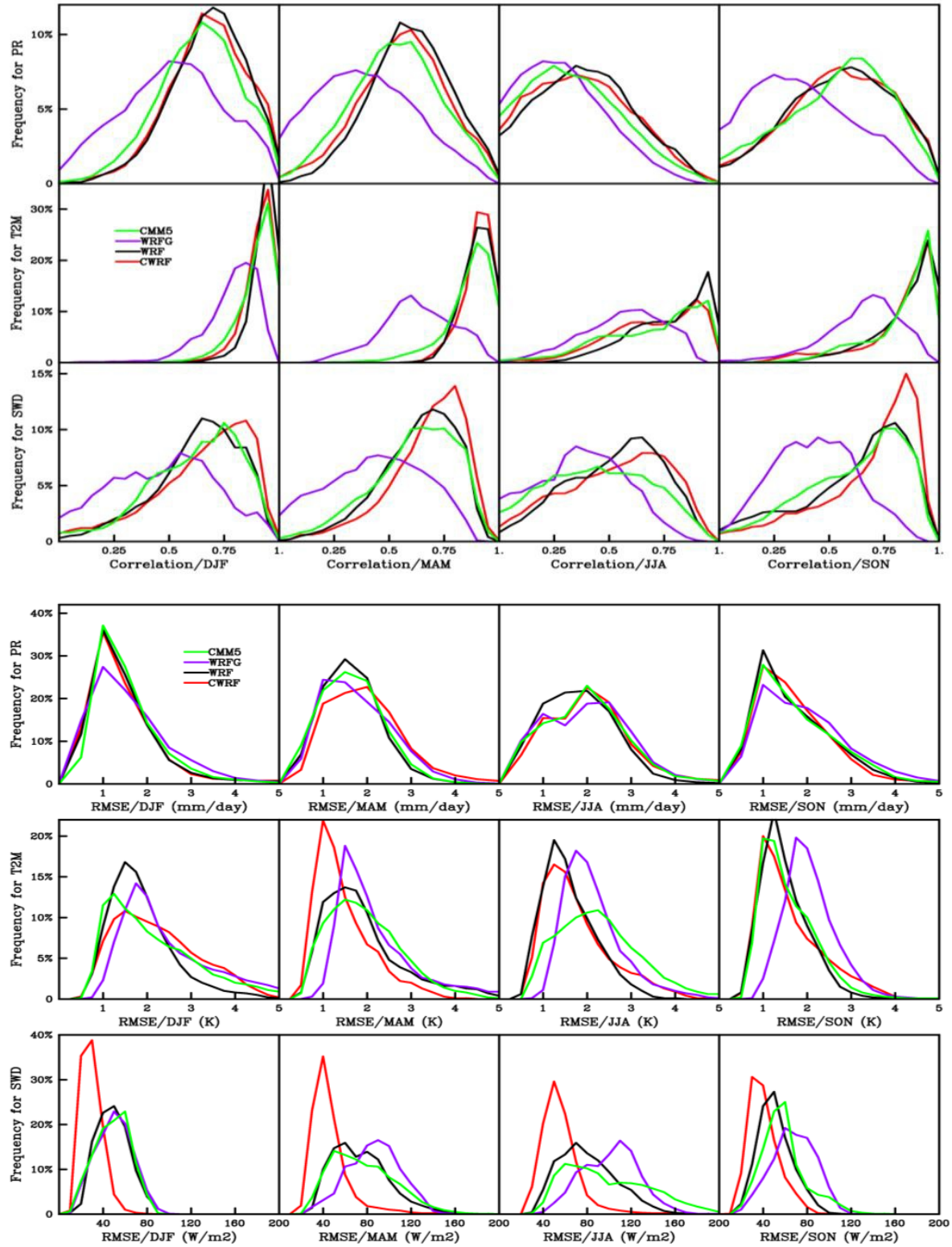

Figure 11. Spatial frequency distributions of correlations (*upper*) and rms errors (*lower*) between simulated (CWRF, WRF, WRFG, CMM5) and observed monthly mean variations of rainfall (PR, mm day^{-1}), surface air temperature (T2M, °C), and surface downwelling shortwave radiation flux (W m^{-2}) in the 4 seasons (DJF, MAM, JJA, SON) during 1982-2004 (1984-2004 for radiation).

Figure 11 compares spatial frequency distributions, for each season, of pointwise correlation coefficients and root-mean-square (rms) errors of precipitation, surface air temperature and downwelling shortwave radiation flux variations during 1982-2004 between observations and simulations by the CWRF, WRF, WRFG, and CMM5. The statistics are based on monthly means for all land grids over the entire inner domain (excluding the buffer zones). As a general rule, the peak frequency occurring more to the right (left) indicates that the respective model simulation has more grids of higher correlations (smaller rms errors) with observations and hence is more realistic overall. The correlations measure the temporal correspondences, while the rms errors depict the magnitude differences, between modeled and observed interannual variations. Clearly, the WRFG performance is the worst by both statistics in all seasons for all the three variables. This may partially result from its use of a coarser horizontal resolution and larger computational domain. For precipitation and temperature, the CWRF and WRF skills are comparable and slightly better than the CMM5. In contrast, for radiation, the CWRF has notable advance to the others throughout the year. This advance is particularly obvious as measured by rms errors.

(c) CWRF/CAR regional climate impact – uncertainty study. Regional climate responses differ substantially among the radiation packages. And the peak frequency occurring more around the zero line indicates that the respective model simulation has more grids of smaller differences from observations and hence is more realistic overall.

Figure 12 compares, among the seven major radiation packages of the original configurations, monthly variations during 2004 of CWRF biases in surface net SW and LW radiative fluxes (NSWS, NLWS) and their CRFs, precipitation, and surface air temperature averaged over the U.S. land. The reference for radiative quantities is from ISCCP, to which the SRB and CERES departures are also given as a measure of observational uncertainty. Both the ensemble mean and min-max range across the packages are presented. The result shows a strong seasonal cycle in the mean NSWS, with systematic underestimates of 10-25 Wm^{-2} in summer due mainly to excessive CRFs, and overestimates of a smaller magnitude in winter. The min-max range exhibits a similar seasonality, about 20 Wm^{-2} in summer and 10 Wm^{-2} in winter. The observational uncertainty, however, is quite large, where SRB and CERES have systematic deficits from ISCCP, with peaks of 15-20 Wm^{-2} in summer. As such, the ensemble mean falls within the observational bound. In contrast, the spread among the radiation packages can be greater than the bound, especially in summer. This is more clearly seen in comparison of spatial root-mean-square errors (rmse, not shown), which are greater in CWRF than those of SRB and CERES throughout the year. For LW, the ensemble captures ISCCP well, where the CRF mean bias is less than 5 Wm^{-2} and NLWS is in between SRB and CERES, while the respective min-max range is about 10 and 5 Wm^{-2}. Consequently, regional climate responses differ substantially among the radiation packages, where the min-

max range is about 0.5 mm day^{-1} for precipitation in summer and about 1 ºC for surface temperature around the year. The precipitation rmse ensemble mean and min-max range also contain a strong seasonal cycle resembling those of SW flux and CRF, while the temperature rmse seasonality is weak just like that of LW flux and CRF.

Figure 13 compares the spatial frequency distributions of CWRF monthly biases during June, July and August 2004 over all the U.S. land grids for the same quantities listed above. These months of the year are identified with maximum model biases and spreads among radiation packages. The peak frequency occurring more around the zero line indicates that the

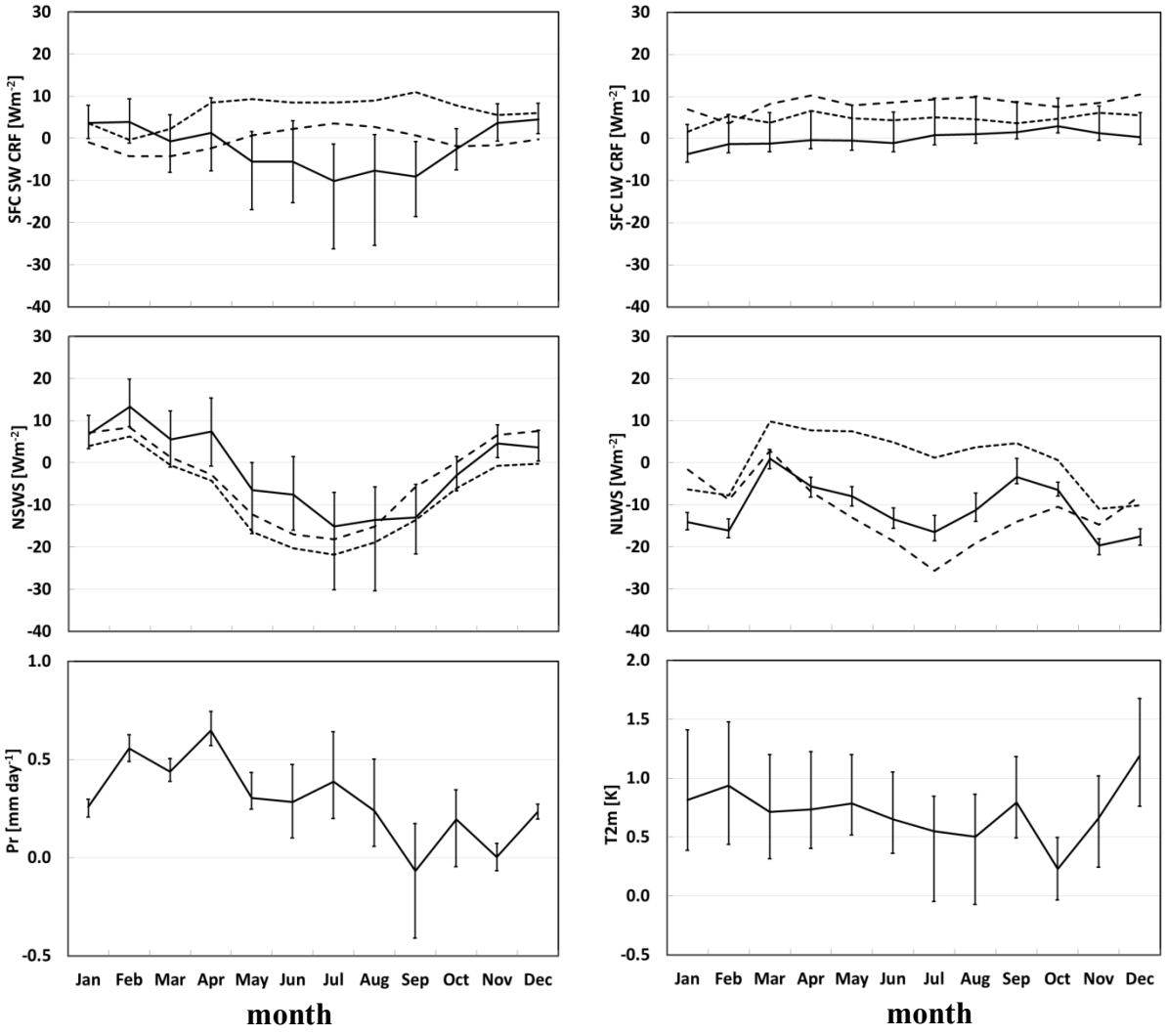

Figure 12. Monthly variations during 2004 of CWRF biases averaged over the U.S. land for surface net SW and LW radiative fluxes and the CRFs (Wm^{-2}), surface air temperature (T2m, K), and precipitation (Pr, mm day^{-1}), including the ensemble mean and min-max range among the 7 major radiation packages. The Reference for radiative quantities is from ISCCP, along with the observational uncertainty shown as the dependences of SRB (dashed) and CERES (dotted).

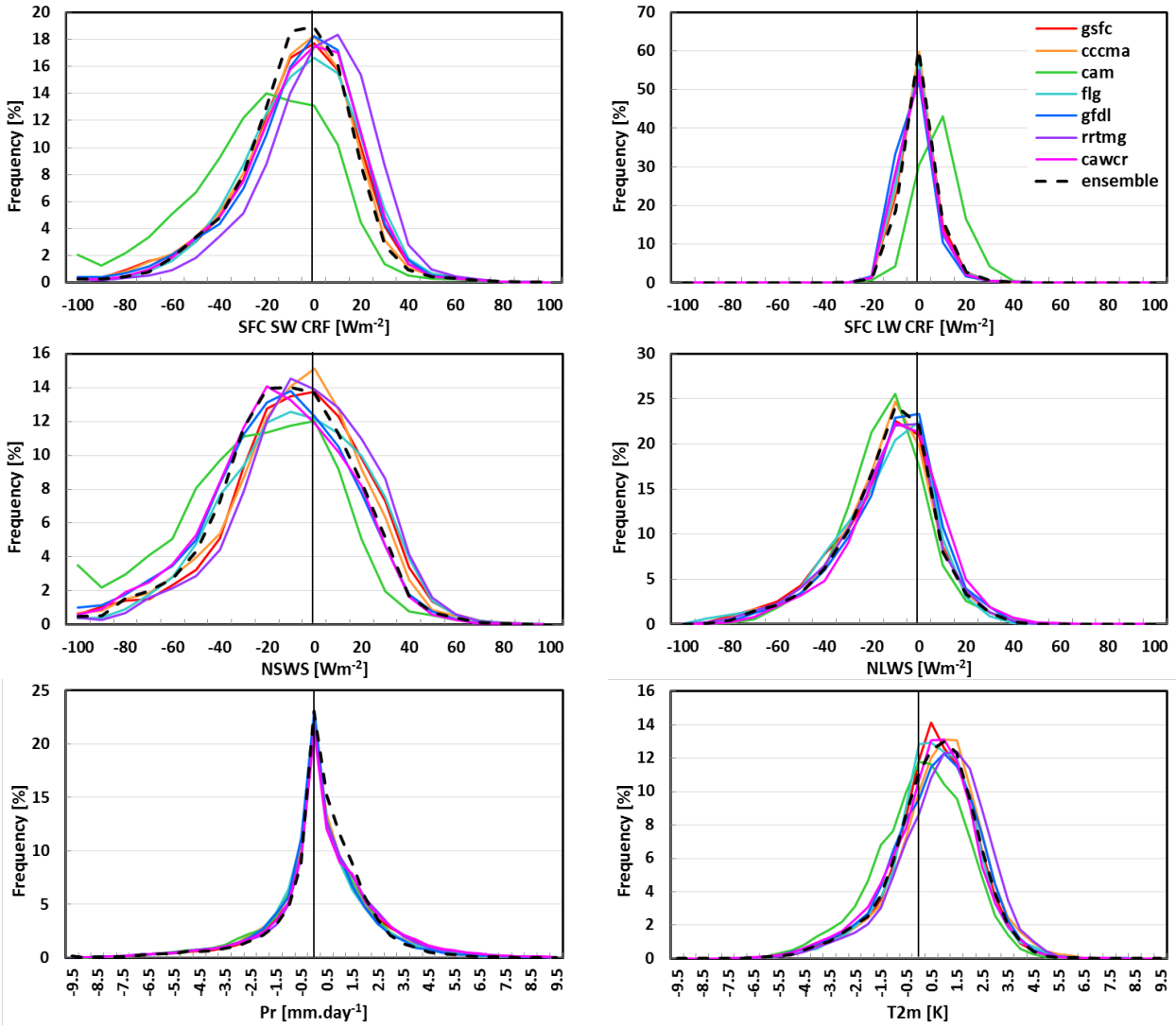

Figure 13. Spatial frequency distributions of CWRF biases in surface net SW (left) and LW (right) radiative fluxes (Top panel), CRFs (middle panel), Pr and T2m (bottom panel) among the 7 major radiation packages. The statistics is based on monthly means during June, July and August 2004 over all U.S. land grids.

respective model simulation has more grids of smaller differences from observations and hence is more realistic overall. Except for precipitation, all other variables show important contrasts among the packages. Clearly, *cam* is an outlier, with its distributions skewed far away from the zero line, indicating more frequent occurrences of larger negative biases in NSWS, NLWS, and SW CRF but opposite biases in LW CRF. To a lesser degree, *rrtmg* also performs somewhat poorly, with its distribution skewed oppositely from *cam*. As a result, the CWRF simulated surface temperatures are generally warmer by using *rrtmg* than *cam*. The overall CWRF performance is comparable among other five packages. The ensemble mean of all the seven packages tends to reduce the overall biases. But the mean local biases in

radiative quantities are still very large. The ranges between the lower and upper 10th percentiles are -38.3 to +17.8 Wm^{-2} for SW CRF and -48.1 to +22.8 Wm^{-2} for NSWS. The corresponding LW values are -7.6 to +9.0 and -40.2 to +7.3 Wm^{-2}. The resulting biases in regional climate responses are also substantial, with the ranges of -1.63 to +2.24 mm day^{-1} for precipitation and -1.61 to +2.55 ºC for temperature. There remains large room for improvement in cloud, aerosol and radiation representations and their interactions with climate.

6. Dominant roles of subgrid-scale cloud structures in model diversity of cloud radiative effects

Zhang, F., X.-Z. Liang, J. Li, and Q.-C. Zeng, 2013: Dominant roles of subgrid-scale cloud structures in model diversity of cloud radiative effects. *J. Geophys. Res.*, **118**, 7733-7749, DOI: 10.1002/jgrd.50604. This was supported by the DOE project and its key results are described below.

Model diversities in estimated irradiances remain large, reducing our confidence in climate change projection. To evaluate the individual roles of cloud cover fraction, optical properties, subgid structure and gaseous effect, is explored for first time. In our study, the dominant roles of subgrid-scale cloud structures (including vertical overlap and horizontal variability) were demonstrated in general, explaining about 40-75% of the total model spreads. We've also found that model spreads of CREs are very sensitive to cloud cover fractions. Such nonlinear sensitivity can be largely reduced after removing the model difference in the treatments of cloud vertical overlap.

Current model spreads of CREs and radiative fluxes can be dramatically reduced.

Figure 14 shows comparisons of zonal mean TOA/SFC SW/LW CREs among the CAR's seven major radiative transfer schemes for dcop_dovp1 (original), dcop_dovp0, scop_dovp0, scop_sovp0, and scop_sovp1, respectively. Where, TOA: top of atmosphere; SFC: ground surface. The results for July 2004 are shown. Different cloud cover members (*cld1*-*cld14*) generate similar CREs. Here we took *cld1* for example. The CRE is defined as $CRE_{LW,SW} = F^{all}_{LW,SW} - F^{clr}_{LW,SW}$, where F is the net (downward minus upward) flux, clr designates clear skies, all denotes a mixture of clear and cloudy skies.

As shown in Figure 14, for dcop_dovp1 (original), when different radiation algorithms employ different approaches for cloud optical properties and subgrid structures, although the same 3D distributions for cloud cover fraction and water path are used, large inter-model diversities exist for both SW and LW CREs. For SW, the spreads of 25-30 Wm^{-2} are found in both the tropic and middle latitude areas, while for LW, the large diversities are most remarkable for TOA CREs over tropics with ranges about 30 Wm^{-2}. For SFC LW CREs,

since their values of 10-40 Wm^{-2} are quite small, the inter-model differences about 5-10 Wm^{-2} can't be ignored.

In dcop_dovp1, the weakest cloud radiative effects for SW CREs are produced by *cccma* and *gfdl*, while those for TOA LW CREs are from *flg*. By removing the cloud inhomogeneity effects, in dcop_dovp0, these three are just located in the middle of the model ranges with stronger CREs. The increments are ~7 Wm^{-2} for SW CREs and 1-2 Wm^{-2} for TOA LW CREs. We've also found that *flg* has the similar SW CREs as rrtmg, cam and cawcr in dcop_dovp1, indicating the similarity between the mixing overlap (i.e., max-random overlap) among high/middle/low cloud blocks for inhomogeneous clouds (i.e., an inhomogeneity factor = 0.7 was employed) and that among adjacent/non-adjacent layers for homogeneous clouds. In brief, the cloud horizontal variability has large impact on modeled CREs and may on their model spreads.

The scop_dovp0 is the same as dcop_dovp0 except that the same *cop* (i.e., *cop1*) is applied to each radiation code. In scop_dovp0, the 7 radiation codes form two groups. Despite whether the conventional or the McICA method is used, those using the same assumption of maximum/random overlap among adjacent and non-adjacent layers, i.e., *cccma*, *cam*, *gfdl*, *rrtmg* and *cawcr*, converge together, while *flg* has the similar performance as *gsfc* because these two adopt the same mixing overlap among high/middle/low cloud blocks. In each group, the influence of cloud optical properties on model spreads is large. Especially in the tropics, the differences of LW and SW CREs among *cccma*, *cam*, *gfdl*, *rrtmg* and *cawcr* are reduced from more than 20 Wm^{-2} in dcop_dovp0 to about 6-8 Wm^{-2} in scop_dovp0 by using the same *cop* (i.e., *cop1*). In a word, the effects of using the same treatment of cloud optical properties are substantially limited by the different assumptions of cloud vertical overlap, although they are not small as shown in each group.

In scop_sovp0 and scop_sovp1, by eliminating the most disagreement in cloud fields, the model discrepancies in dcop_dovp1 dramatically diminish. Similar SW and LW CREs are shown globally across all seven radiation codes. At most latitudes, model spreads are no more than 5 Wm^{-2}. Cloud radiative effects are much weaker in scop_sovp1 than in scop_sovp0, illustrating the horizontal inhomogeneity effects. Clearly, the large existing inter-model discrepancies in CREs primarily come from different cloud treatments that are originally adopted by different radiation codes.

Obviously, even today there exist significant discrepancies among different cloud schemes, inferring our current limited understandings of cloud radiative effects. By removing the difference in clouds, we have successfully reduced the model discrepancies in cloud radiative effects, even smaller than the inter-observation uncertainty.

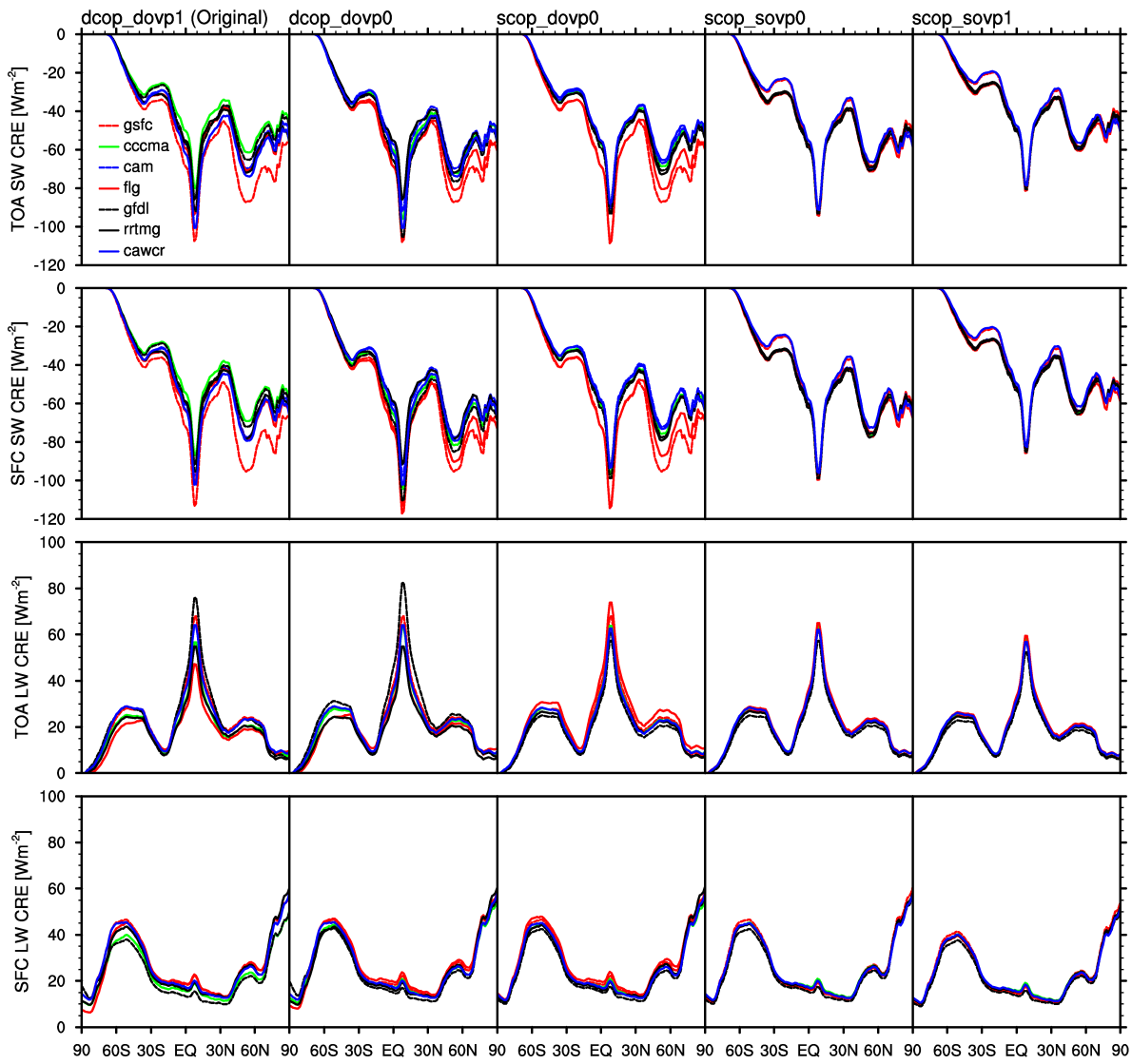

Figure 14. Comparisons of zonal mean TOA/SFC SW/LW CRE [Wm^{-2}] among the CAR's major radiative transfer schemes for dcop_dovp1 (original), dcop_dovp0, scop_dovp0, scop_sovp0, and scop_sovp1. Where, TOA: top of atmosphere; SFC: ground surface. Here, the results are for July 2004, and we took the combination of *Xu and Randall* [1996] for stratiform and *Slingo* [1987] for deep convective cloud cover fractions for example.

We demonstrated dominant roles of cloud subgrid structure in model diversities.

The percentages of the model diversities contributed by different treatments for different factors are concluded in Table 5. As cloud fields become similar, the inter-model discrepancies, as well as the min-max ranges among 14 cloud cover members (*cld1-cld14*), are significantly reduced, even to smaller than the corresponding inter-observation ranges. Different treatments of cloud inhomogeneity effect account for 19.5-44.2% of inter-model diversities, as indicated by the reduction of the medians from 10-14 Wm^{-2} in dcop_dovp1 to

7-8 Wm^{-2} in dcop_dovp0. As shown in our results, in dcop_dovp1, based on the same 3D distributions for cloud condensate and cloud cover fraction, using the mixing overlap among adjacent/non-adjacent layers for inhomogeneous clouds generally produce weakest SW CREs and smallest SWUPT, e.g., *cccma* and *gfdl*. And both can be enhanced by removing the cloud inhomogeneity effects in dcop_dovp0, which then decreases the model spreads. Moreover, using the similar cloud optical properties seems to have no positive effects on the reduction of the SW model discrepancies, although it reduces the min-max ranges of ~7 Wm^{-2} in dcop_dovp0 to < 5 Wm^{-2} in scop_dovp0. In scop_dovp0, two groups are formed based on the different assumptions of cloud vertical overlap: one, *cccma*, *cam*, *gfdl*, *rrtmg* and *cawcr*, and the other, *flg* and *gsfc*. In each group, different *cops* largely contribute to the current inter-model spreads. Taking *cccma*, *cam*, *gfdl*, *rrtmg*, and *cawcr* for example, using the same *cop* (i.e., *cop1*) decreases the model spreads among them from 4.33-7.06 Wm^{-2} and 5.09-9.05 Wm^{-2} in dcop_dovp0 to 1.87-3.28 Wm^{-2} and 1.50-3.73 Wm^{-2} in scop_dovp0 for TOA SW CREs and SWUPT, respectively. However, such roles are greatly limited by the variety in existing assumptions of cloud vertical overlap originally adopted by different radiation codes. Furthermore, when the same treatment of cloud vertical overlap is consistently applied in scop_sovp0, both the medians and the min-max ranges are greatly reduced. All the medians (i.e., inter-model discrepancies) further decrease to <3-4 Wm^{-2} for CREs and SWUPT and <7 Wm^{-2} for SWDNS, and all the min-max ranges are < 2-3 Wm^{-2}. Those model spreads are even smaller than their corresponding inter-observation ranges. Hence, the dominant role of cloud vertical overlap is demonstrated in general as the key contributor not only to the current model diversities (44.4-50.6%) but also to the sensitivity of model ranges to different *clds* (i.e., min-max ranges) except SWDNS. For SWDNS, in scop_sovp0 and scop_sovp1, all radiation codes converge together except *gsfc* (not shown). The specific performance of *gsfc* may result from the simple scaling method to include the CO_2 effects on SWDNS [*Chou and Suarez*, 1999], which partly compensates the contribution from the different treatments of cloud vertical overlap. In gas_exp, by removing the discrepancies caused by the different gas absorptions of CH_4, CO_2, N_2O and O_2, the medians are generally smaller than those in scop_sovp1, especially for SWDNS. This indicates that the uncertainties in gas SW absorptions still remain large, playing substantial roles in model spreads of SWDNS (~17.5%). In summary, for SW, about 50-75% of the current model disagreement results from the different treatments of cloud subgrid structures.

For LW, the different cloud subgrid structures usually account for 40-67% of the inter-model discrepancies, playing the dominant roles. For TOA LW CREs, the substantial impacts (16.4%) of cloud optical properties are limited and suppressed by the variety in the existing assumptions of cloud vertical overlap. As shown in our results, in scop_dovp0, two groups are formed, although they are not as distinct as those for SW. The model spread among *cccma*, *gfdl*, *rrtmg*, and *cawcr* that adopt the same assumption of max-random overlap among

adjacent/non-adjacent layers of homogeneous clouds decrease from 3.94-7.97 Wm^{-2} in dcop_dovp0 to 2.64-3.28 Wm^{-2} in scop_dovp0. For LWDNS, different gas absorptions of CH_4, N_2O, and CFCs explain 17.9% of its inter-model diversity. And different cloud inhomogeneity effects are found to be critical to model ranges of SFC LW CREs and LWDNS (34-39%). Based on the same 3D distributions for cloud condensate and cloud cover fraction, the radiation schemes using the mixing overlap among adjacent/non-adjacent layers for inhomogeneous clouds generally produce weakest LW SFC CREs and smallest LWDNS in dcop_dovp1, such as *cccma* and *gfdl*. Both can be enhanced in dcop_dovp0 by removing the cloud inhomogeneity effects (not shown).

Table 5. The percentage of the model diversities contributed by different treatments for different factors [%] [a]

factors	TOA CRE		SFC CRE		UPT		DNS	
	SW	LW	SW	LW	SW	LW	SW	LW
cloud subgrid variability	35.4	3.3	19.5	38.9	36.0	25.6	44.2	34.2
cloud vertical overlap	44.4	36.9	44.4	27.9	50.6	0.1	8.4	13.5
cloud optical properties (including particle effective size)	-	16.4	-	-	-	-	-	-
trace gaseous effects (i.e., CO_2, O_2, CH_4, and N_2O for SW; CH_4, N_2O, CFCs, etc. for LW)	1.2	3.1	3.3	1.9	-	6.4	17.5	17.9

[a] Here,

UPT: upward fluxes at TOA

DNS: downward fluxes at SFC

Negative percentages are not shown due to the negative effects.

We reduced current nonlinear sensitivity of model spreads to cloud fractions.

Figure 15 is to quantitatively compare the inter-model discrepancy across the CAR's seven major radiation transfer codes of the global mean TOA SW CRE, SWUPT, SFC SW CRE, and SWDNS (SW downward fluxes at surface) among different sets of experiments. The medians and min-max ranges are among 14 inter-model discrepancies generated by applying the same cloud cover member (*cld1-cld14*) to each intercomparison of the CAR's seven major radiation transfer codes. "obs" denotes the inter-observation range among ISCCP, SRB, CERES and CERES_EBAF. The results for July 2004 are shown. Note that to simplify the following descriptions, the median is used to show the general inter-model discrepancy

for each set of experiments.

The complicated nonlinear nature existing in the coupling of cloud/radiation processes is highlighted in this study. The current inter-model diversities among different radiation codes vary strongly with different cloud cover members (*clds*, Figure 15), and meanwhile the

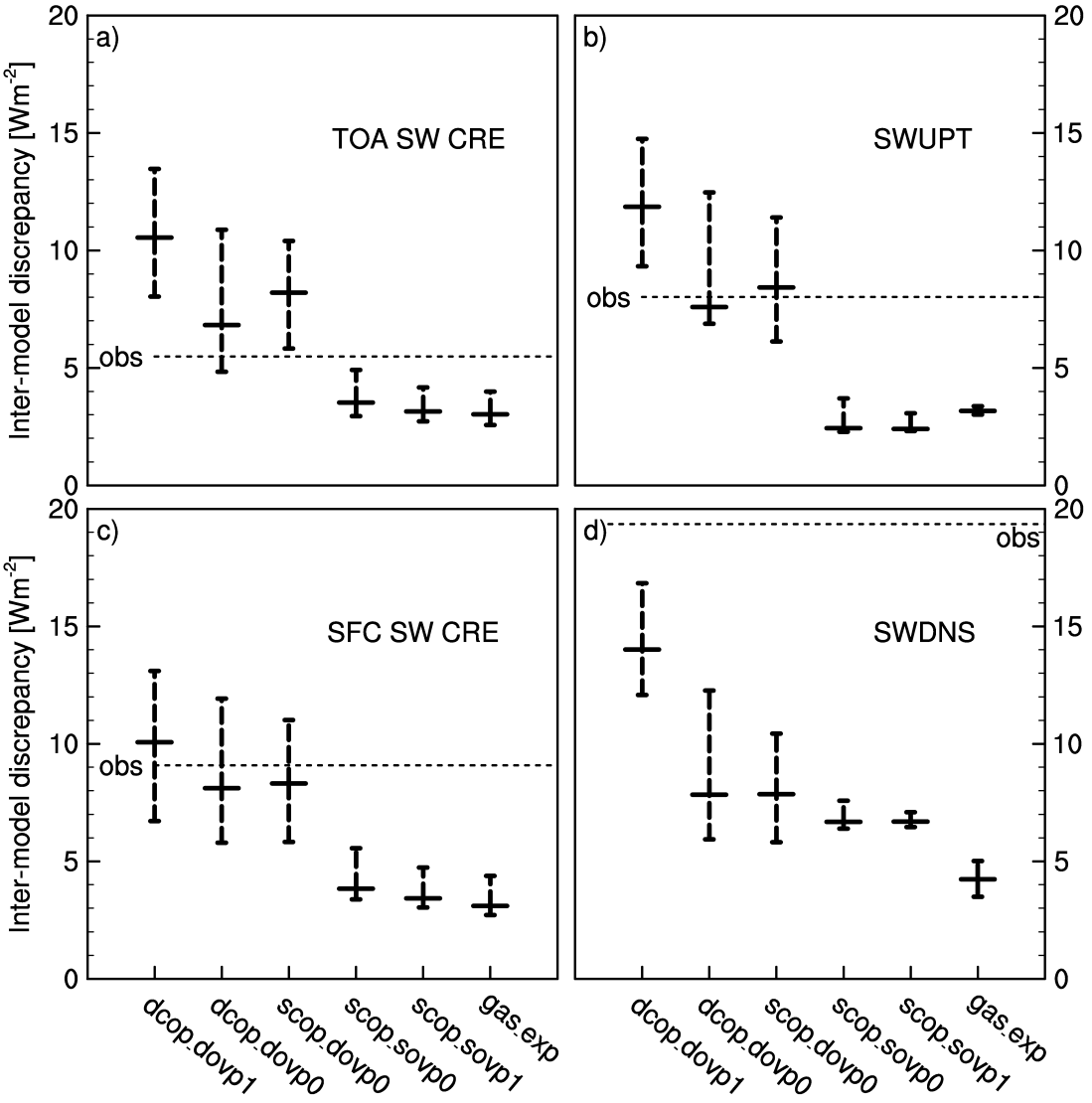

Figure 15. Comparisons of the inter-model discrepancy across the CAR's seven major radiation transfer codes of the global mean a) TOA SW CRE; b) SWUPT; c) SFC SW CRE; d) SWDNS among different sets of experiments. The medians and min-max ranges are among 14 inter-model discrepancies generated by applying the same cloud cover member (*cld1-cld14*) to each intercomparison of the CAR's seven major radiation transfer codes. "*obs*" denotes the inter-observation uncertainty among ISCCP, SRB, CERES and CERES_EBAF. The results are for July 2004.

dependences both of the existing inter-cld discrepancies and of the inter-cop discrepancies are also shown on different radiation transfer codes (not shown). The major reasons have been investigated in this study. In general, using the different assumptions of cloud vertical overlap accounts for most the sensitivity of the inter-model diversity to different *clds*. Different *clds* produce different vertical profiles of cloud cover fractions, which determine whether the different assumptions of cloud vertical overlap matters much for radiation. So different *clds* produce quite different ranges of clear-sky portions among different radiation codes, and then generate the nonlinear sensitivity. Moreover, for SW CREs/TOA LW CREs, the nonlinear sensitivities of inter-cld spreads to host models mainly result from the different cloud optical properties used, and for SFC LW CREs, applying different cloud inhomogeneity effects is the major reason. Both two factors are closely related to cloud optical properties, indicating the strong nonlinear influences of cloud cover fractions and cloud optical properties on the radiative transfer calculations. Using the different cloud subgrid-scale structures explains well the sensitivities of inter-cop discrepancies to host radiation codes for SW CREs. In a word, by removing the contributions from the different treatments of some key cloud factors mentioned above, the remaining nonlinear effects between cloud and radiation are largely reduced.

REFERENCE

Barker, H.W., and Coauthers, 2003: Assessing 1D atmospheric solar radiative transfer models: Interpretation and handling of unresolved clouds. *J. Climate*, **16**, 2676-2699.

Chou, M.-D., and M.J. Suarez, 1999: A solar radiation parameterization for atmospheric studies. [Last revision on March 2002] *Technical Report Series on Global Modeling and Data Assimilation*, M.J. Suarez (Ed.), NASA/TM-1999-104606, Vol. 15, Goddard Space Flight Center, Greenbelt, MD, 42 pp.

Chou, M.-D., M.J. Suarez, X.-Z. Liang, and M.M.-H. Yan, 2001: A thermal infrared radiation parameterization for atmospheric studies. [Last revision on July 2002] Technical Report Series on Global Modeling and Data Assimilation, M.J. Suarez (Ed.), NASA/TM-2001-104606, Vol. 19, Goddard Space Flight Center, Greenbelt, MD, 56 pp.

Clough, S.A., M.W. Shephard, E.J. Mlawer, J.S. Delamere, M.J. Iacono, K. Cady-Pereira, S. Boukabara, P.D. Brown, 2005: Atmospheric radiative transfer modeling: A summary of the AER codes. *J. Quant. Spectrosc. Radiat. Transfer*, **91**, 233-244.

Collins, W.D., and Coauthers, 2004: Description of the NCAR Community Atmosphere Model (CAM 3.0), NCAR Technical Note, NCAR/TN-464+STR, 226 pp.

Dobbie, J., J. Li, and P. Chýlek, 1999: Two- and four-stream optical properties for water clouds and solar wavelengths. *J. Geophys. Res.*, **104**, 2067-2079.

Ebert, E.E. and J.A. Curry, 1992: A parameterization of cirrus cloud optical properties for climate models. *J. Geophys. Res.*, **97**, 3831-3836.

Edwards, J. M., S. Havemann, J. C. Thelen, and A. J. Baran, 2007: A new parameterization for the radiative properties of ice crystals: Comparison with existing schemes and impact in a GCM. *Atmos. Res.*, **83**, 19-35.

Ferrier, B. S., Y. Lin, T. Black, E. Rogers, and G. DiMego, 2002: Implementation of a new grid-scale cloud and precipitation scheme in the NCEP Eta model. Preprints, 15th Conference on Numerical Weather Prediction, San Antonio, TX, *Amer. Meteor. Soc.*, 280-283.

Freidenreich, S.M., and V. Ramaswamy, 1999: A new multiple-band solar radiative parameterization for general circulation models. *J. Geophys. Res*., **104**, 31389–31409.

Fu, Q., and K.N. Liou, 1992: On the correlated k-distribution method for radiative transfer in nonhomogeneous atmospheres. *J. Atmos. Sci.*, **49**, 2139-2156.

Fu, Q., and K.N. Liou, 1993: Parameterization of the radiative properties of cirrus clouds. *J. Atmos. Sci.*, 50, 2008-2025.

Fu, Q., 1996: An accurate parameterization of the solar radiative properties of cirrus clouds for climate models. *J. Climate*, **9**, 2058-2082.

Fu, Q., K.N. Liou, M.C. Cribb, T.P. Charlock, A. Grossman, 1997: Multiple scattering parameterization in thermal infrared radiative transfer. *J. Atmos. Sci.*, **54**, 2799-2812.

Fu, Q., P. Yang, and W.B. Sun, 1998: An accurate parameterization of the infrared radiative properties of cirrus clouds for climate models. *J. Climate*, **11**, 2223-2237.

Gu, Y. and K.N. Liou, 2006: Cirrus cloud horizontal and vertical inhomogeneity effects in a GCM. *Meteorl. Atmos. Phys.*, **91**, 223-235.

Gu, Y., K. N. Liou, S. C. Ou, and R. Fovell, 2011: Cirrus cloud simulations using WRF with improved radiation parameterization and increased vertical resolution. *J. Geophys. Res.*, **116**, doi:10.1029/2010JD014574.

Hu, Y. X., and K. Stamnes, 1993: An accurate parameterization of the radiative properties of water clouds suitable for use in climate models. *J. Climate*, **6**, 728-742.

Iacono, M.J., J.S. Delamere, E.J. Mlawer, M.W. Shephard, S.A. Clough, and W.D. Collins, 2008: Radiative forcing by long-lived greenhouse gases: Calculations with the AER radiative transfer models. *J. Geophys. Res.*, **113**, D13103, doi: 10.1029/2008JD009944.

IPCC (Intergovernmental Panel on Climate Change), 2007: Climate Change 2007: The Physical Science Basis. S. Solomon, D. Qin, M. Manning, M. Marquis, K. Averyt, M.M.B. Tignor, H.L. Miller, Jr., and Z. Chen (eds.), Contribution of Working Group I to the Fourth Assessment Report of the IPCC. Cambridge University Press, New York.

Kahn, R.A., B.J. Gaitley, J.V. Martonchik, D.J. Diner, K.A. Crean, and B. Holben, 2005: Multiangle Imaging Spectroradiometer (MISR) global aerosol optical depth validation based on 2 years of coincident Aerosol Robotic Network (AERONET) observations. *J. Geophys. Res.*, **110**, D10S04, doi:10:1029/2004JD004706.

Kahn, R.A., M.J. Garay, D.L. Nelson, K.K. Yau, M.A. Bull, B.J. Gaitley, J.V. Martonchik, and R.C. Levy, 2007: Satellite-derived aerosol optical depth over dark water from MISR and MODIS: Comparisons with AERONET and implications for climatological studies. *J. Geophys. Res.*, **112**, D18205, doi:10.1029/2006JD008175.

Key, J., 2001: Streamer User's Guide. Cooperative Institute for Meterological Satellite Studies, University of Wisconsin, 96 pp.

Kiehl, J.T., J.J. Hack, G.B. Bonan, B.A. Boville, B.P. Briegleb, D.L. Williamson, and P.J. Rasch, 1996: Description of the NCAR Community Climate Model (CCM3). NCAR Tech. Note NCAR/TN-420+STR, 143 pp. [Available from Publications Office of NCAR, P.O. Box 3000, Boulder, CO 80307.]

Kristjässon, J.E., J.M. Edwards, D.L. Mitchell, 1999: A new parameterization scheme for the optical properties of ice crystals for use in general circulation models of the atmosphere. *Phys. Chem. Earth*, **B24**, 231-236.

Li, J., 2002: Accounting for unresolved clouds in a 1D infrared radiative transfer model. Part I: Solution for radiative transfer, including cloud scattering and overlap. *J. Atmos. Sci.*, **59**, 3302-3320.

Li, J. and H. W. Barker, 2005: A radiation algorithm with correlated-k distribution, Part I: local thermal equilibrium. *J. Atmos. Sci.*, **62**, 286-309.

Lindner, T.H., and J. Li, 2000: Parameterization of the optical properties for water clouds in the infrared. *J. Climate*, **13**, 1797-1805.

Liou, K.N., Y. Gu, Q. Yue, and G. McFarguhar, 2008: On the correlation between ice water content and ice crystal size and its application to radiative transfer and general circulation models. *Geophys. Res. Lett.*, **35**, L13805, doi:10.1029/2008GL033918.

Martin, G. M., D. W. Johnson, and A. Spice, 1994: The measurement and parameterization of effective radius of droplets in warm stratocumulus clouds. *J. Atmos. Sci.*, **51**, 1823-1842.

McFarquhar, G.M., 2000: Comments on 'Parameterization of effective sizes of cirrus-cloud particles and its verification against observations' by Zhian Sun and Lawrie Rikus (October B, 1999, 125, 3037-3055). *Quart. J. Roy. Meteor. Soc.*, **127**, 261-266.

Meinshausen, M., S.J. Smith, K. Calvin, J.S. Daniel, M.L.T. Kainuma, J-F. Lamarque, K. Matsumoto, S. Montzka, S. Raper, K. Riahi, A. Thomson, G.J.M. Velders, D.P. van Vuuren, 2011: The RCP greenhouse gas concentrations and their extension from 1765 to 2500. *Climatic Change*, **109**, 213–241.

Min, Q.L., and L.C. Harrison, 1996: Cloud properties derived from surface MFRSR measurements and comparison with GOES results at the ARM SGP site. *Geophys. Res. Lett.*, **23**, 1641-1644.

Morcrette, J.J., H.W. Barker, J.N.S. Cole, M.J. Iacono, and R. Pincus, 2008: Impact of a new radiation package, McRad, in the ECMWF integrated forecasting system. *Mon. Wea. Rev.*, **136**, 4773–4798.

Oreopoulos, L., and E. Mlawer, 2010: The continual intercomparison of radiation codes (CIRC): Assessing anew the quality of GCM radiation algorithms. *Bull. Amer. Meteor. Soc.*, **91**, 305-310, doi:10.1175/2009BAMS2732.1.

Oreopoulos, L., and Coauthers, 2012: The continual intercomparison of radiation codes: results from phase I. *J. Geophys. Res.*, **117**, D06118, doi: 10.1029/2011JD016821.

Savijärvi, H., Arola, A. and Räisänen, P., 1997: Short-wave optical properties of precipitating water clouds. *Quart. J. Roy. Meteorol. Soc.*, **123**, 883–899.

Schwarzkopf, M.D., and V. Ramaswamy, 1999: Radiative effects of CH_4, N_2O, halocarbons and the foreign-broadened H_2O continuum: A GCM experiment. *J. Geophys. Res.*, **104**, 9467–9488.

Slingo, J. M., 1987: The development and verifcation of a cloud prediction scheme for the ECMWF model. *Quart. J. Roy. Meteorol. Soc.*, **113**, 899-927.

Slingo, A. S., 1989: A GCM parameterization for the shortwave radiative properties of water clouds. *J. Atmos. Sci.*, **46**, 1419-1427.

Stackhouse, Jr., Paul W., Shashi K. Gupta, Stephen J. Cox, Taiping Zhang, J. Colleen Mikovitz, and Laura M. Hinkelman, 2011: The NASA/GEWEX Surface Radiation Budget Release 3.0: 24.5-Year SRB Data set Released. *GEWEX News*, **21**, No. 1, February, 10-12.

Sun, Z.A., and L. Rikus, 1999: Parametrization of effective radius of cirrus clouds and its verification against observations. *Q. J. Royal. Meteor. Soc.,* **125**, 3037-3056.

Sun, Z., 2008: Development of the Sun-Edwards-Slingo Radiation Scheme (SES2). CAWCR Technical Report No. 009, Centre for Australian Weather and Climate Research, Australian Bureau of Meteorology, 94pp.

Szczodrak, M., P.H. Austin, and P.B. Krummel, 2001: Variability of optical depth and effective radius in marine stratocumulus clouds. *J. Atmos. Sci.*, **58**, 2912.2926.

Uppala, S.M., D.P. Dee, S. Kobayashi, P. Berrisford, and A.J. Simmons, 2008: Towards a climate data assimilation system: Status update of ERA-Interim. *ECMWF Newsletter*, **115,** 12–18.

Wielicki, B. A., B. Barkstrom, E. F. Harrison, R. Lee, G. Smith, and J. Cooper, 1996: Clouds and the Earth's Radiant Energy System (CERES): An Earth observing system experiment. *Bull. Am. Meteorol. Soc.*, **77**, 853 – 868.

Xu, K.-M., and D.A. Randall, 1996: A semiempirical cloudiness parameterization for use in climate models. *J. Atmos. Sci.*, **53**, 3084-3102.

Yu, H., Y. J. Kaufman , M. Chin , G. Feingold, L. A. Remer, T. L. Anderson, Y. Balkanski, N. Bellouin, O. Boucher, S. Christopher, P. DeCola, R. Kahn, D. Koch, N. Loeb, M. S. Reddy, M. Schulz, T. Takemura, and M. Zhou, 2006: A review of measurement-based assessments of the aerosol direct radiative effect and forcing. *Atmos. Chem. Phys.*, **6**, 613-666.

Zhang, Y.-C., W. B. Rossow, A. A. Lacis, V. Oinas, and M. I. Mishchenko, 2004: Calculation of radiative fluxes from the surface to top-ofatmosphere based on ISCCP and other global datasets: Refinements of the radiative transfer model and the input data. *J. Geophys. Res.*, **109**, D19105, doi: 10.1029/2003JD004457.

ABBREVIATIONS AND ACRONYMS

AER	Atmospheric and Environmental Research
AEROCOM	Aerosol comparisons between observations and models
AOD	Aerosol Optical Depth
ARM	Atmospheric Radiation Measurement
CAM	NCAR Community Atmosphere Model
cam	the radiation transfer scheme from CAM
CAR	Cloud-Aerosol-Radiation Ensemble Modeling System
CAWCR	the Centre for Australia Weather and Climate Research
cawcr	the radiation transfer scheme from CAWCR
cbl	scheme for boundary cloud fraction
ccb	scheme for convective cloud cover fraction
CCCMA	Canadian Centre for Climate Modeling and Analysis
cccma	the radiation transfer scheme from CCCMA
cci	scheme for cirrus fraction
ccs	scheme for stratiform cloud cover fraction
CERES	Cloud and the Earth's Radiant Energy System
CHARTS	Code for High resolution Accelerated Radiative Transfer and Scattering
CIRC	Continual Intercomparison of Radiation Codes
CMM5	climate extension of MM5
CRE	Cloud Radiative Effect
CRF	Cloud Radiative Forcing
CSSP	Conjunctive Surface-Subsurface Process Model
ctot	scheme for horizontal total cloud cover fraction
CWRF	Climate extension of the Weather Research and Forecasting model
cwp	cloud water path
dei	scheme for cloud ice effective particle size
DJF	December-January-Febuary
DOE	U.S. Department of Energy
EBAF	Energy Balanced and Filled
ECMWF	European Centre for Medium-Range Weather Forecasts
ECP	Ensemble Cumulus Parameterization
ERI	the Global Interim ECMWF Reanalysis

flg	Fu-Liou-Gu radiation transfer scheme, considering cloud horizontal variability
flg_homo	Fu-Liou-Gu radiation transfer scheme for homogeneous clouds
GCM	General Circulation Model
GEWEX	Global Energy and Water Cycle Experiment
GFDL	NOAA's Geophysical Fluid Dynamics Laboratory
gfdl	radiation transfer scheme from GFDL
GHG	GreenHouse Gas
GSFC	NASA's Goddard Space Flight Center
gsfc	the radiation transfer scheme from GSFC with Liang's modifications
IPCC	Intergovernmental Panel on climate Change
ISCCP	International Satellite Cloud Climatology Project
IWC	ice water content
JJA	June-July-August
LBL	Line-by-line
LBLRTM	Line-by-line radiative transfer model
LW	longwave
LWC	liquid water content
lwi	scheme for LW cloud ice optical property
lwl	scheme for LW cloud liquid optical property
lwr	scheme for cloud rain water LW optical properties
LWUPT	LW upwelling fluxes at TOA
LWDNS	LW downwelling fluxes at SFC
MAM	March-April-May
McICA	Monte-Carlo Independen Column Approximation
MISR	Multi-angle Imaging SpectroRadiometer
MODIS	Moderate Resolution Imaging Spectroradiometer
NASA	National Aeronautics and Space Administration
NCAR	National Center for Atmospheric Research
NCEP	National Centers for Environmental Prediction
NLWS	NET LW fluxes at SFC
NOAA	National Oceanic and Atmospheric Administration
NSWS	NET SW fluxes at SFC
Pr	precipitation
rad	radiation transfer scheme
rad_ext	one external module for radiation package
RCM	Regional Climate Model
RCP	Representative Concentration Pathway
RCP8.5	Rising radiative forcing pathway to 8.5 Wm-2 in 2100

RCP6.0	Stabilization radiative forcing pathway to 6.0 Wm-2 in 2100
RCP4.5	Stabilization radiative forcing pathway to 4.5 Wm-2 in 2100
RCP2.6	Strong mitigation radiative forcing pathway to 2.6 Wm-2 in 2100 and decline
rel	scheme for cloud liquid effective particle radius
rmse	Root Mean Square error
rrtmg	AER Rapid Radiative Transfer Model for application to GCMs
SFC	Ground Surface
SON	September-October-November
SRB	NASA/GEWEX Surface Radiation Budget
SW	Shortwave
swl	schemes for cloud liquid water SW optical properties
swi	schemes for cloud ice water SW optical properties
swr	schemes for cloud rain water SW optical properties
SWUPT	SW upwelling fluxes at TOA
SWDNS	SW downwelling fluxes at SFC
T2m	air temperature at 2m
TOA	Top of Atmosphere
WRF	Weather Research and Forecasting model
WRFG	earlier WRF version 2 with some extensions